Chapter 4

Microanalysis results

4.1 Metallographic analysis

At first the samples of the considered titanium composite have been analysed by mean of optical microscope, to verify the presence of eventual defects on the observed surfaces. In fact especially the grain morphology and the matrix status around the fibers results interesting to analyse, to foreseen immediately problems that could expand during the work condition, cause the aforesaid defects. For this reason the observing surfaces have been polished and then chemically attacked by Kroll solution.

About the composite produced by *HIP* process, the metallographic images show an uniform part around the fiber.

Fig.1 Metallographic images 10x of Ti6Al4V-SiC_f

About this zone, the disposition of the grains formed during the fabrication diffusion process results homogeneous and devoid of harmful empty micro-space. This situation is even clearer in the following Fig.2.

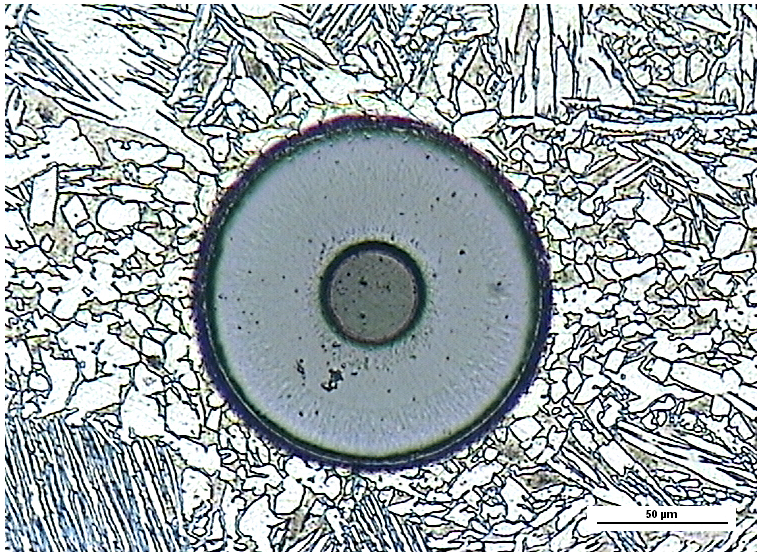

Fig.2 Metallographic images 20x of Ti6Al4V-SiC_f

About the matrix characteristic, it results constituted by grains with not homogeneous form. It is possible to note this in Fig.1, on the superior and inferior parts than the fiber layer. This forms are observable also about the images carried out on the parallel sections to the major axis of the fiber (Fig.4).

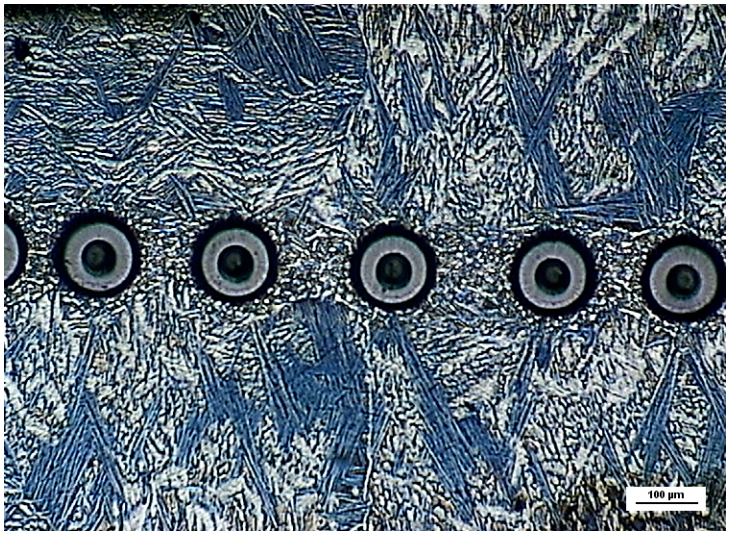

Fig.3 Metallographic images 5x of Ti6Al4V-SiC_f

The particular matrix structure is probably due to cooling step of the *HIP* fabrication process, during that the rapid cooling cause the observed forms, that however do not affect negatively the composite general behaviour.

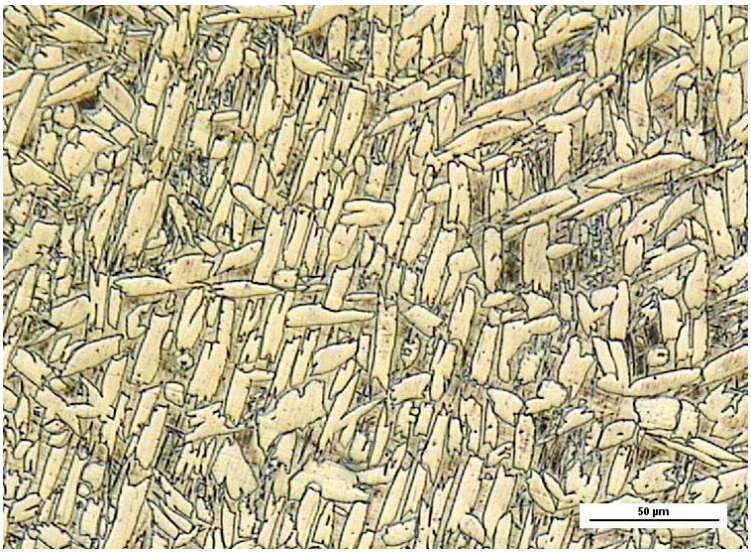

Fig.4 Metallographic images 20x of Ti6Al4V-SiC_f, parallel section to the fiber axis

In particular it results interesting to note the difference between the matrix form in the composite and that obtaining in the simple Ti6Al4V alloy by the same metallographic method (Fig.5). In fact in the two cases especially the α phase (clearer grains) results having a different form, cause the aforesaid reasons.

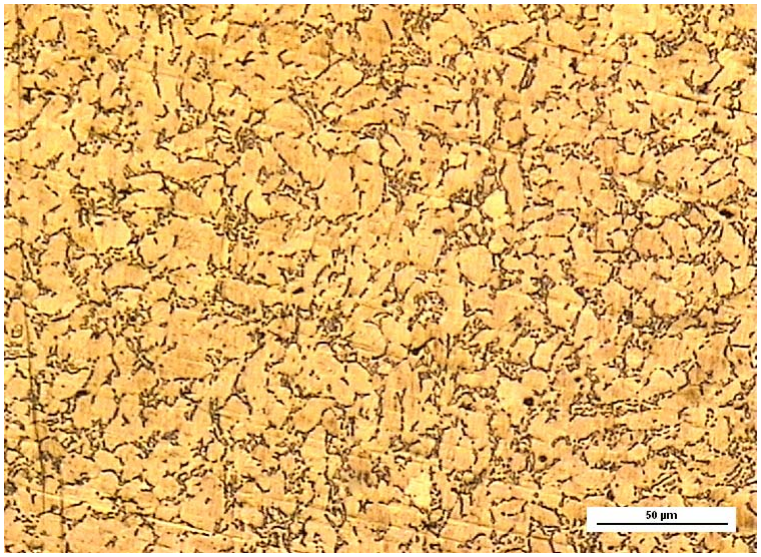

Fig.5 Metallographic images 20x of Ti6Al4V alloy

The composite produced by *RDB* process has been observed, too. By the same metallographic methodologies, especially the cross section to the fibers has been observed (Fig.6).

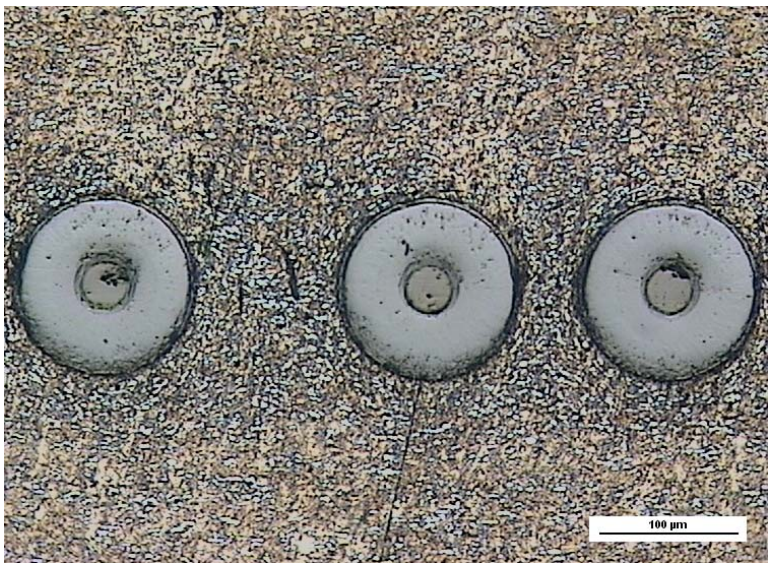

Fig.6 Metallographic images 10x of Ti6Al4V-SiC_f produced by Roll Diffusion Bonding

At once it is possible to observed the clean difference about the matrix form. In particular the grains result smaller and with more homogeneous form than the grains obtained in the *HIP* process, cause probably to the fast time process in *RDB*.

Fig.7 show the full-bond and complete interfaces recrystallisation of the metal flowed between the fibres [12].

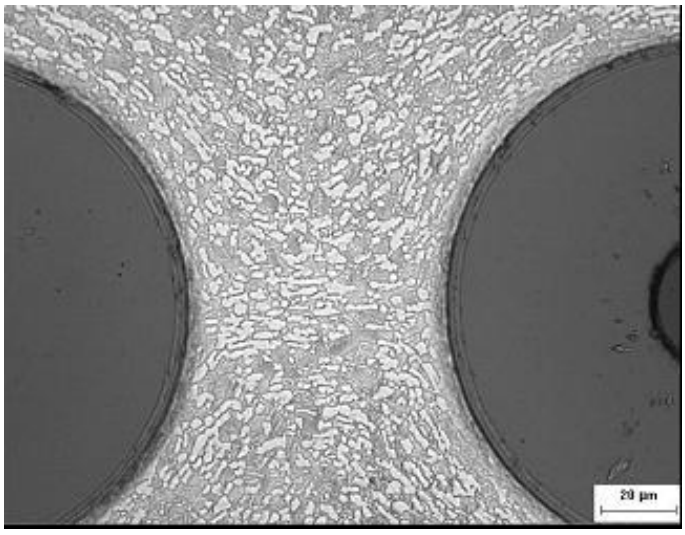

Fig.7 Particular of the matrix formed between the fibers in RDB composite

But through a more careful observation of the analyzed sections, some defects in the interfacial zones are notable (indicated in Fig.8).

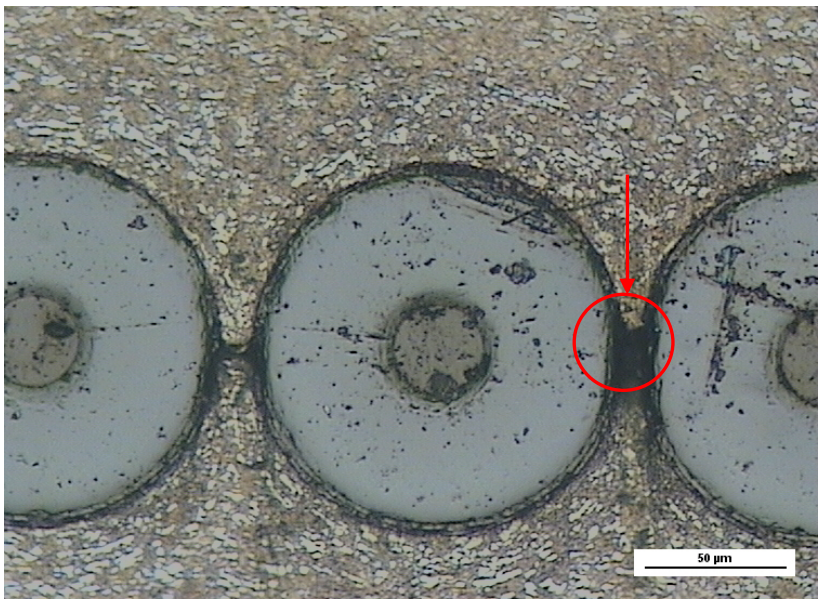

Fig.8 Particular defects notable about RDB composite

In fact difficulties about the matrix uniform flow have been noticed between the fiber that are the most near. This aspect will be studied in depth by very attention, because this empty micro-space can result very harmful about the composite application.

4.2 SEM/EDS analysis

The EDS analysis has been fundamental to a first evaluation of concentration for the most significant elements. Fig.9 shows the SEM image of a sample prepared as described in Fig.5 in Cap.3. Ten EDS measurements, from P1 to P10, have been carried out along the direction indicated by the arrow; the distance between each test position is 10 µm. The element concentrations are displayed in Fig.10.

Results can be summarized as follows:

1- Si is found in graphite (P3-P9),
2- Si signal disappears at the graphite-matrix boundary,
3- there is a transition region where progressively the signal of carbon decreases while that of titanium increases (P8-P10).

To obtain a better resolution, an acceleration voltage of 12 kV has been used, lower with respect to operating conditions normally employed. Under these conditions, the diameter of interaction volume is 1.5 µm for matrix and 4 µm for carbon fiber.

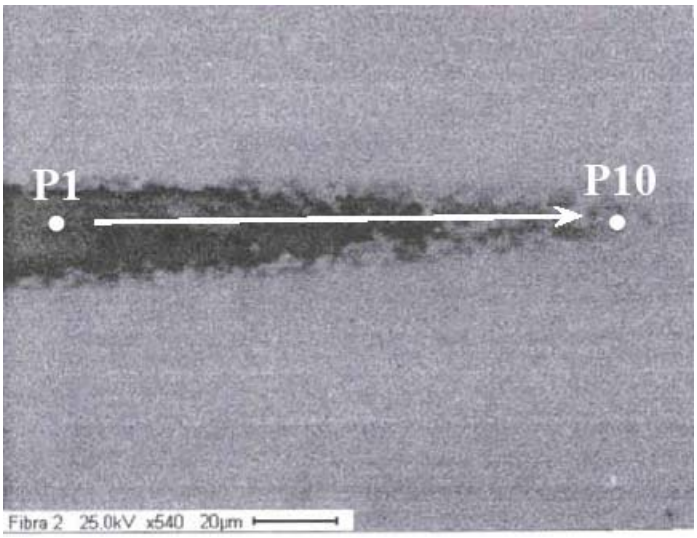

Fig.9 As-fabricated composite: SEM micrograph of a fiber-matrix zone. The arrow indicates the direction along which EDS measurements have been performed

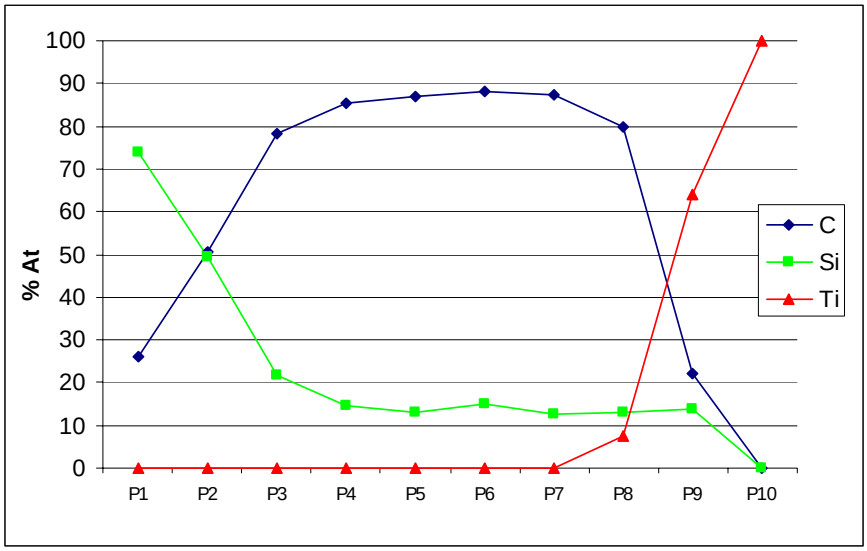

Fig.10 Elemental concentration profiles measured by EDS microanalysis

The resolution is not very high, however sufficient to avoid experimental artefacts in determining concentration profiles.

The calculus of the interaction volume in this case is very important to determinate the test reliability, especially in this material where there are more layer of two different sub-materials (matrix and fiber) along the low depth. The dimensions for the interaction volume (in terms of diameter *d* and depth z_{max}) is given by following formula:

$$d(\mu m) = 0{,}231 * (E_0^{3/2} - E_c^{3/2}) / \rho$$

$$z_{\max}(\mu m) = 0{,}033 * (E_0 - E_c)^{1{,}67} A / \rho Z$$

with E_o incident electron energy associated to the survey voltage, A atomic weight of the element, ρ volumetric mass in g/cm^3, E_c chemical potential of the element and Z atomic number for the element. For the measurements along the aforesaid direction, in Tab.1 the calculated results are showed.

	z_{max} (μm)	d (μm)
P1	1,46	3,98
P2	1,56	4,07
P3	1,68	4,17
P4	1,71	4,19
P5	1,72	4,19
P6	1,67	4,16
P7	1,72	4,19
P8	1,55	3,87
P9	0,67	2,16
P10	0,41	1,55

Tab.1 Interaction volumes for the EDS measurements

A second EDS analysis has been carried out at three different potential in every point to verify and to calculate the influence of this interaction volume about the aforesaid test (Fig.11). The results are showed in Fig.12 and in Tab.2.

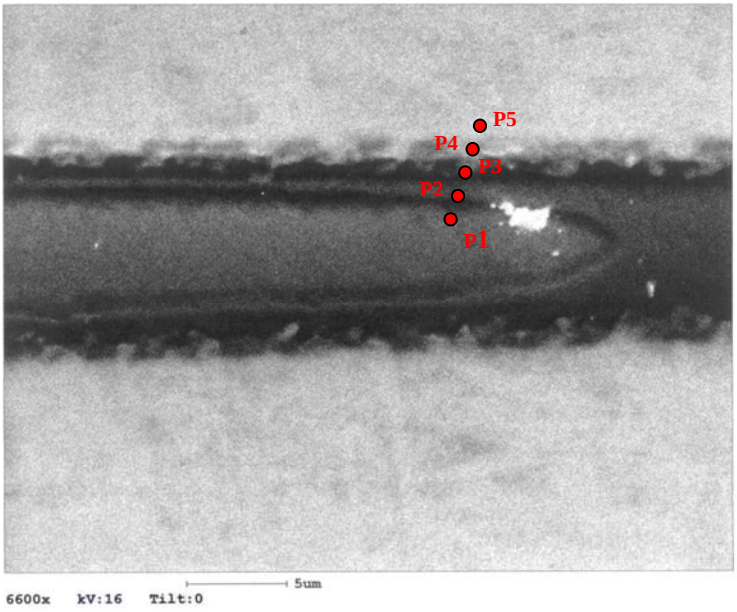

Fig.11 As-fabricated composite: SEM micrograph of a fiber-matrix zone and second direction for the EDS measurements

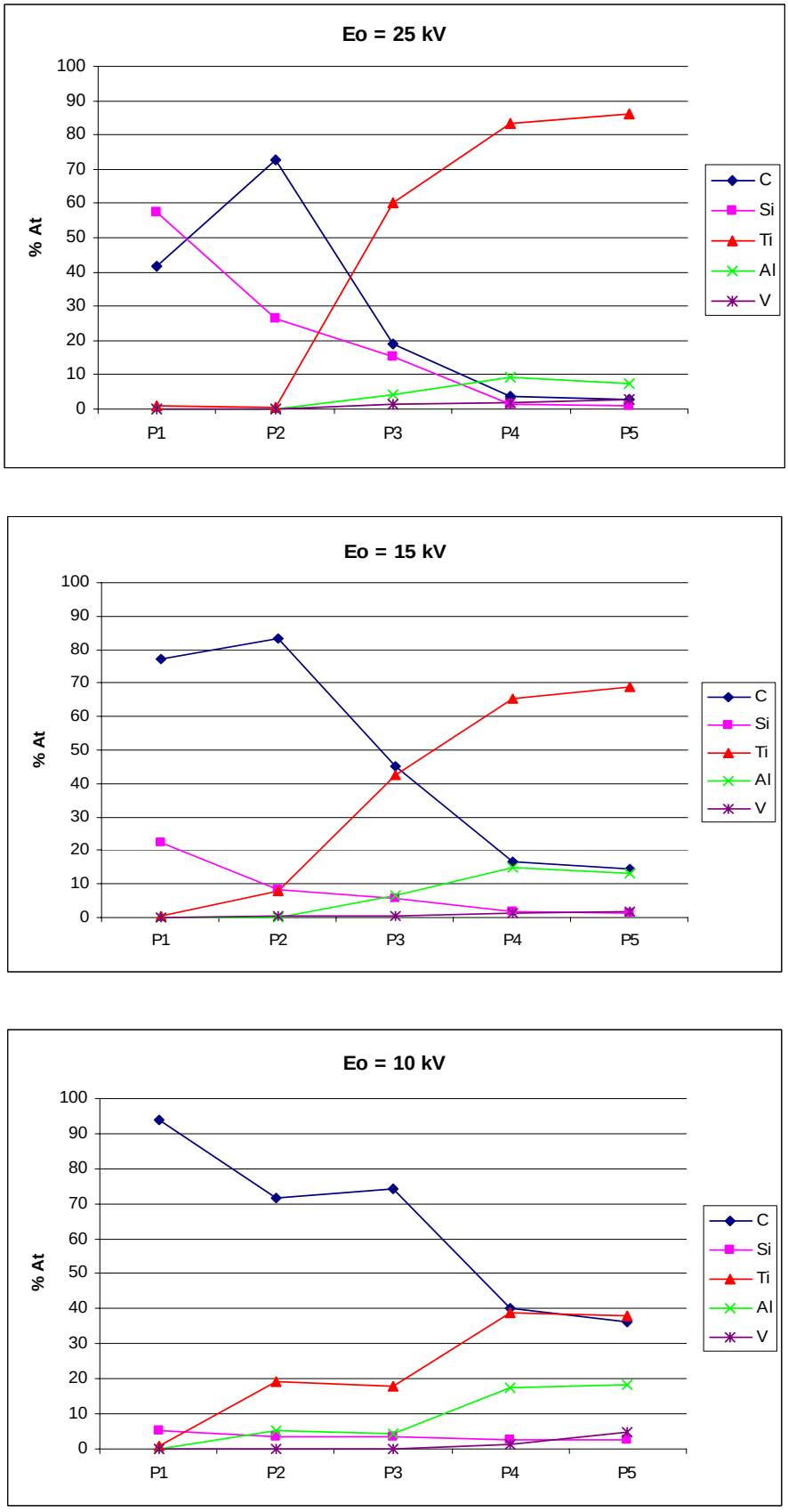

Fig.12 Element concentration profiles measured by EDS microanalysis

P1	E_0 (kV)	z_{max} (μm)	d (μm)
	25	5,68	12,32
	15	2,47	5,82
	10	1,26	3,16
P2			
	25	5,95	12,56
	15	2,3	5,39
	10	0,93	2,54
P3			
	25	3,22	7,41
	15	2,1	5,06
	10	0,95	2,60
P4			
	25	2,60	6,24
	15	2,10	5,36
	10	0,63	1,97
P5			
	25	2,55	6,15
	15	1,02	2,97
	10	0,6	1,91

Tab.2 Interaction volumes for the EDS measurements in fig.14

The SEM/EDS analysis has been carried also the RDB composite, in order to have a first description about the diffusion profiles of the main elements (C, Si and Ti)on the fibre-matrix interface [12]. The results are reported in Fig.13, where the concentration profile in a particular part of the aforesaid interface is considered.

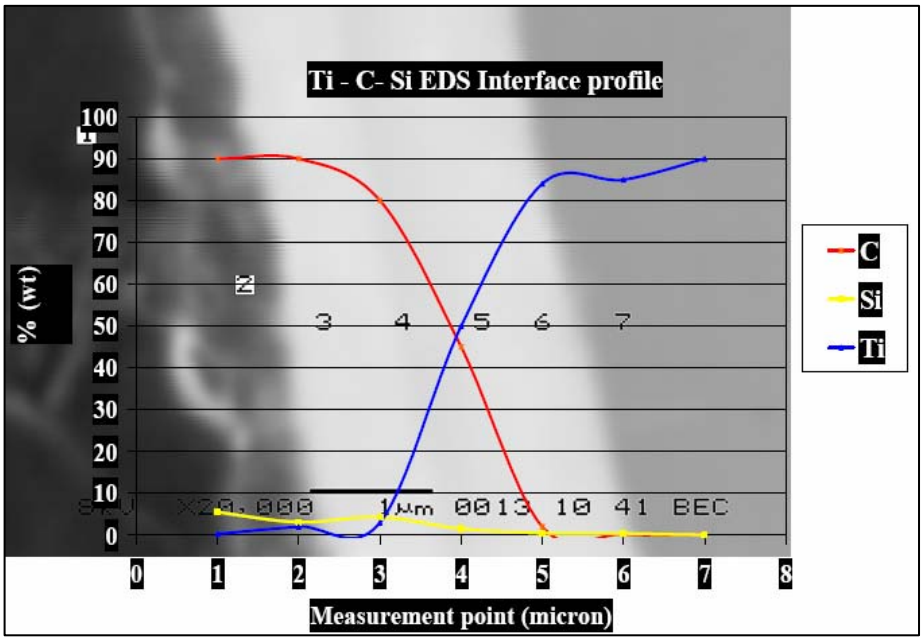

Fig.13 Element concentration profiles measured by EDS microanalysis on the RDB composite [12]

4.3 AES analysis

4.3.1 Zone 1

A first evaluation (Fig.15-16-17) of the present elements has been done in the interface zone indicated in Fig.14 by Auger spectroscopy. About the as-fabricated sample, not only the presence of the aforesaid element is confirmed, but a not negligible quantity of oxygen.

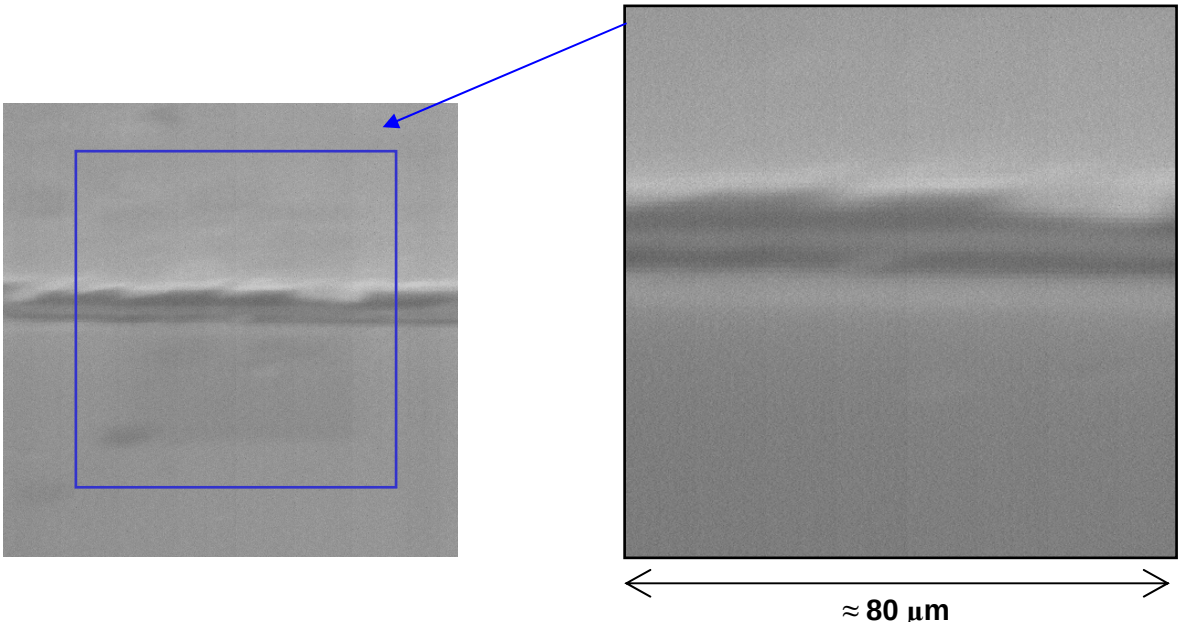

Fig.14 Examination site for the AES measurements

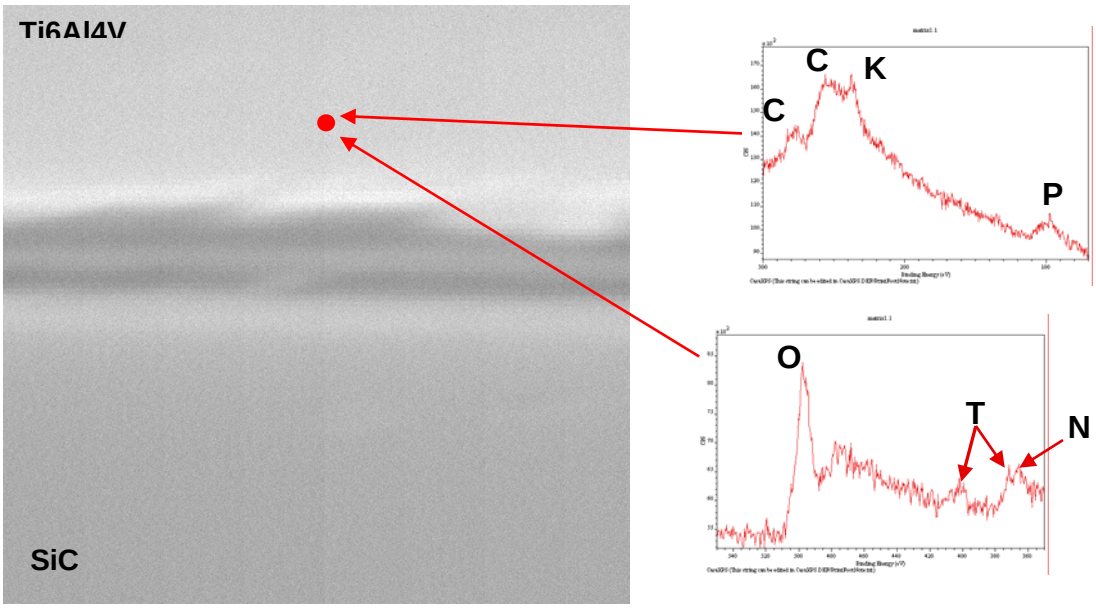

Fig.15 First AES observations about as-fabricated sample

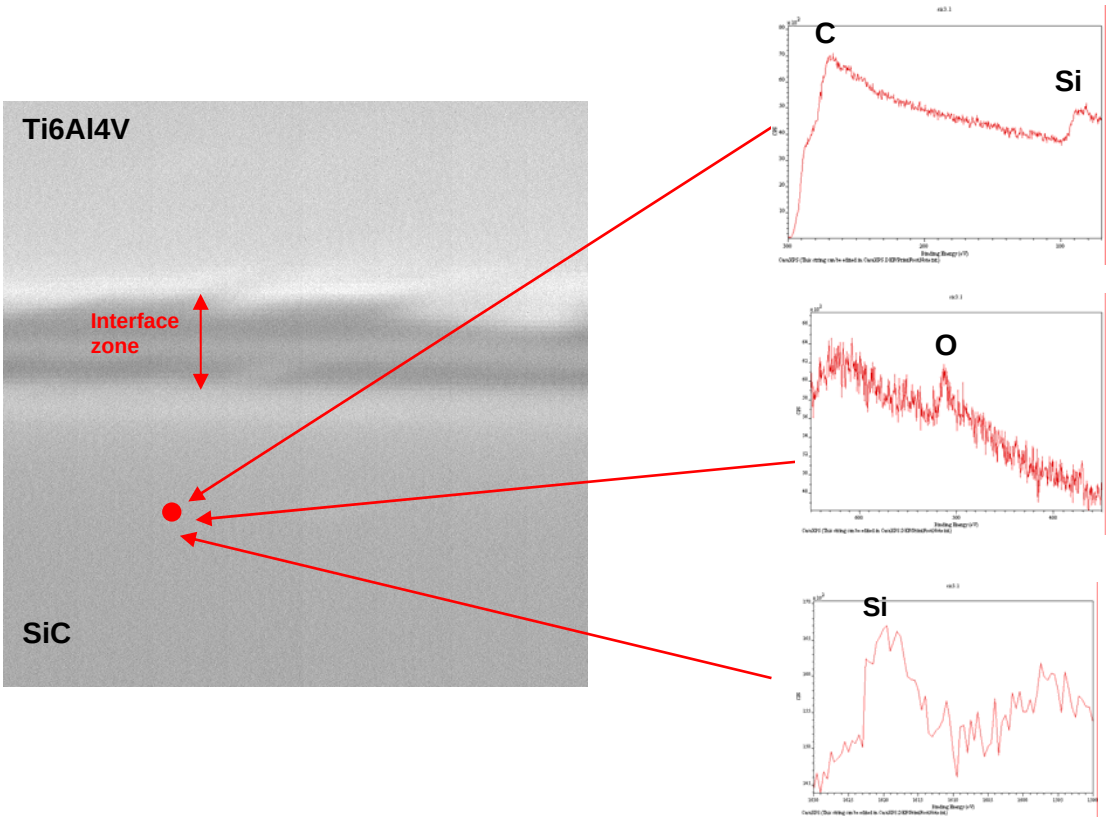

Fig.16 First AES observations about as-fabricated sample

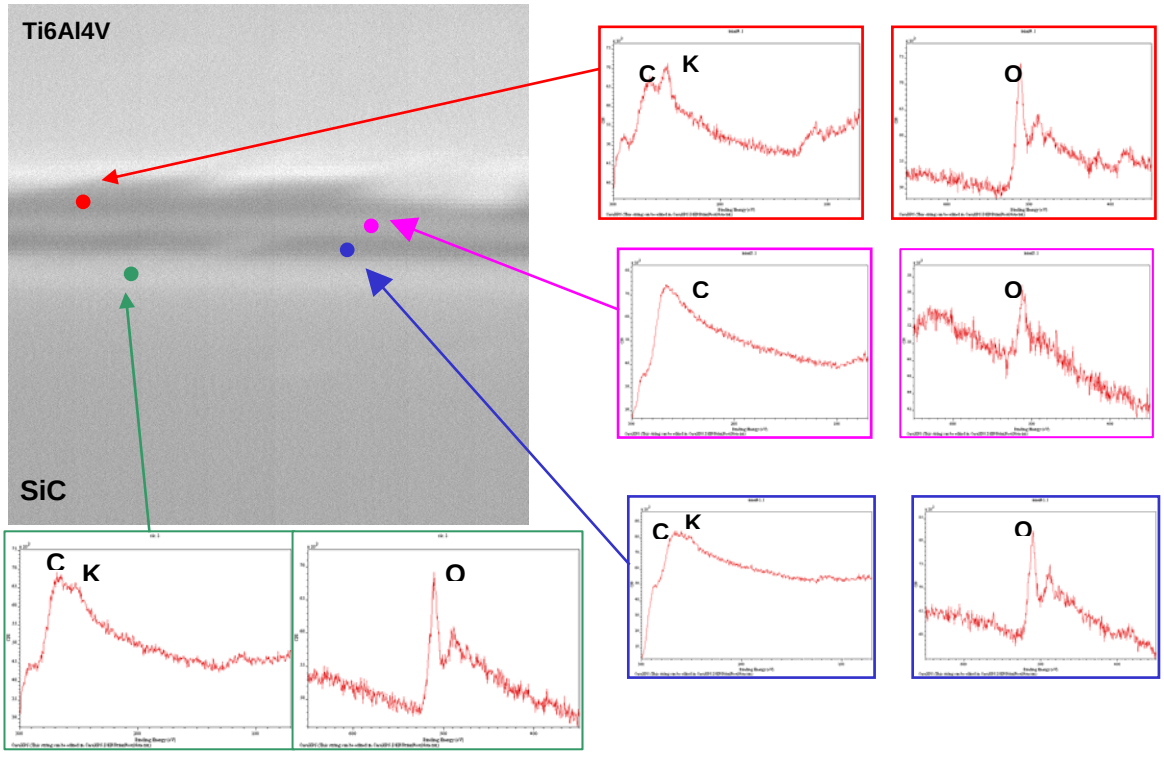

Fig.17 AES observations about as-fabricated sample on the fiber/matrix interface

The analysis of the as-fabricated sample has highlighted contaminating elements calcium and potassium (Fig.15 and Fig.17): calcium is in the matrix, while potassium sin in the fiber-matrix interface and in a small part on SiC. Then, variable quantity of oxygen is present on every part of the sample.

Now it's possible to value the results about the heat treated sample, in particular that subjected to T = 600 °C and t = 1000h, i.e. the more extreme case, to verify at once the differences with the as fabricated case.

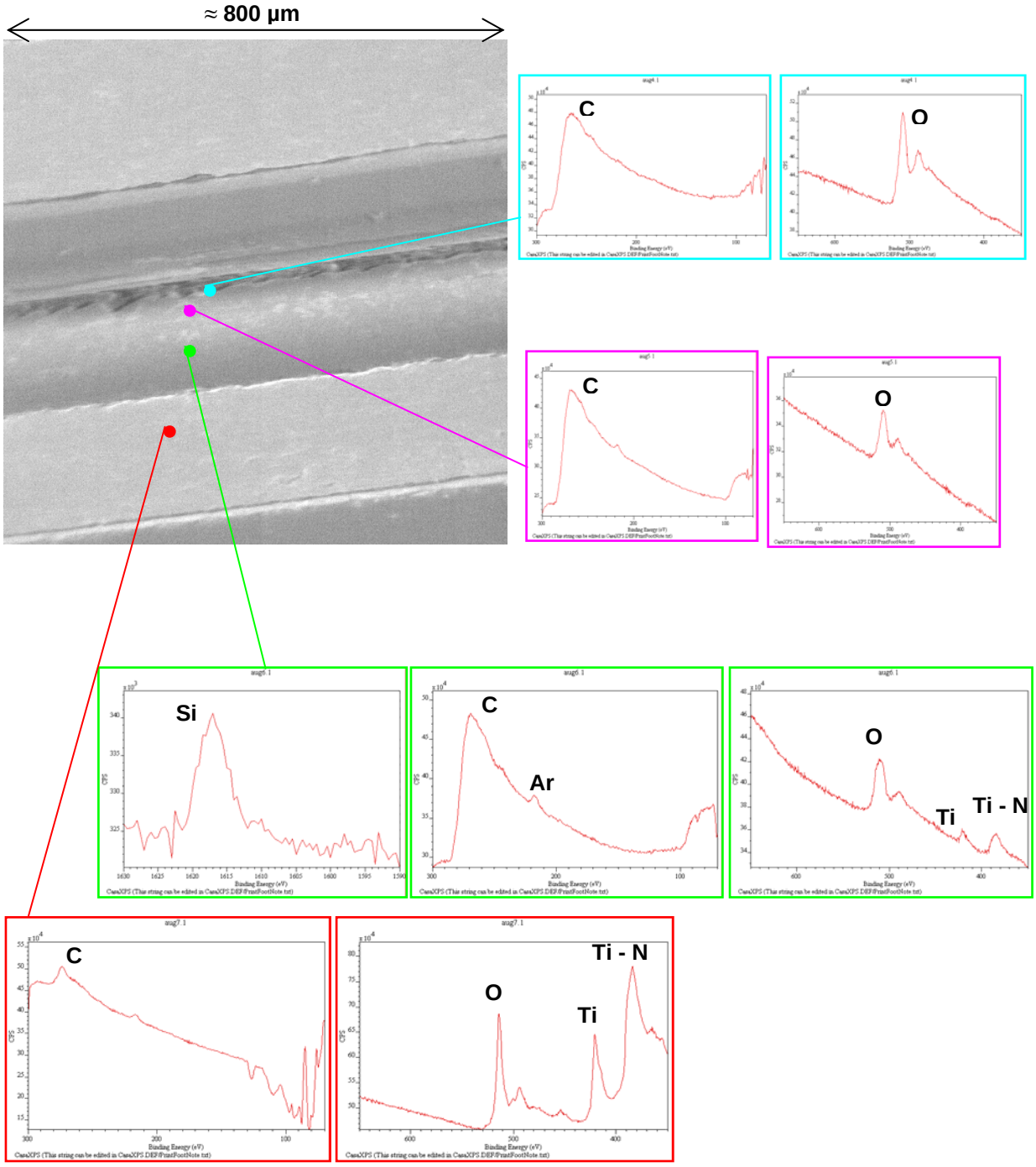

Fig.18 AES observations on the fiber/matrix interface about the sample treated to 600°C and 1000 h

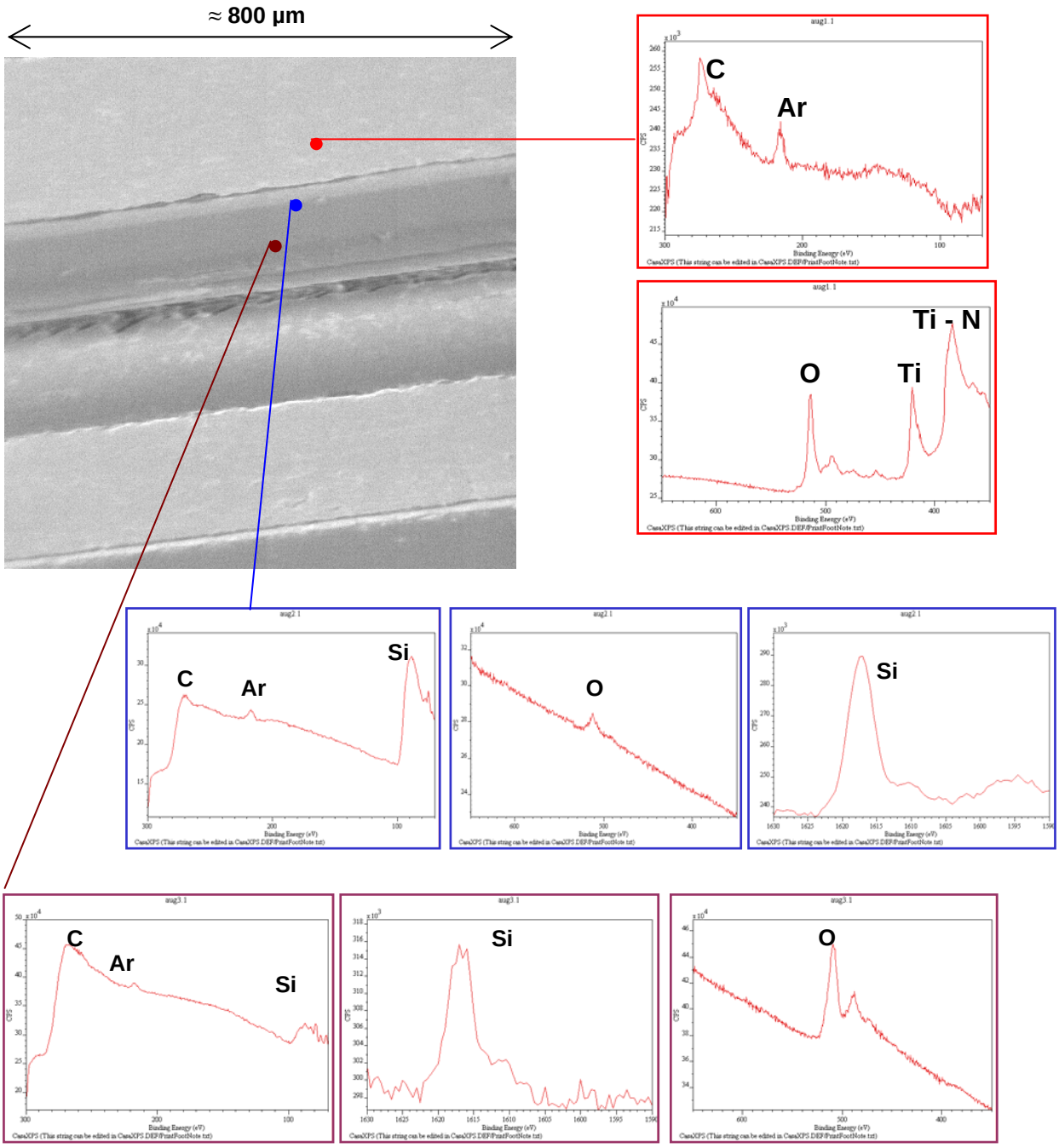

Fig.19 Other AES AES observations on the fiber/matrix interface about the treated sample

Considering smaller observation zones, it's possibile to have the measurements showed in Fig.20 e Fig.21:

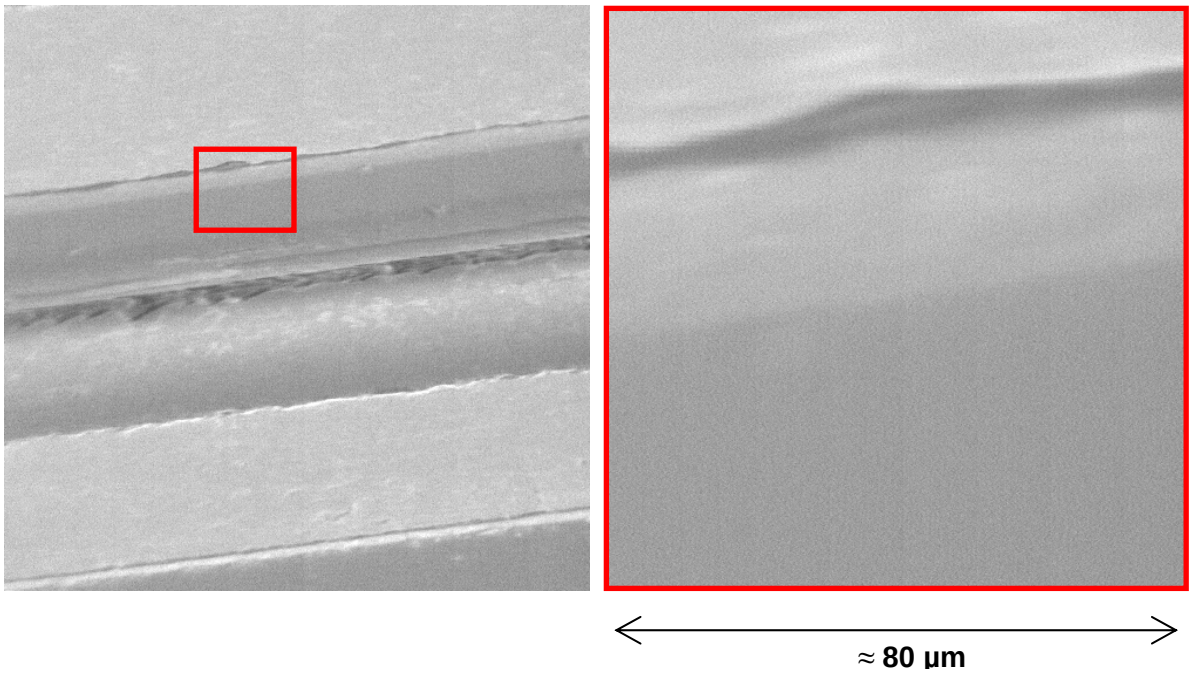

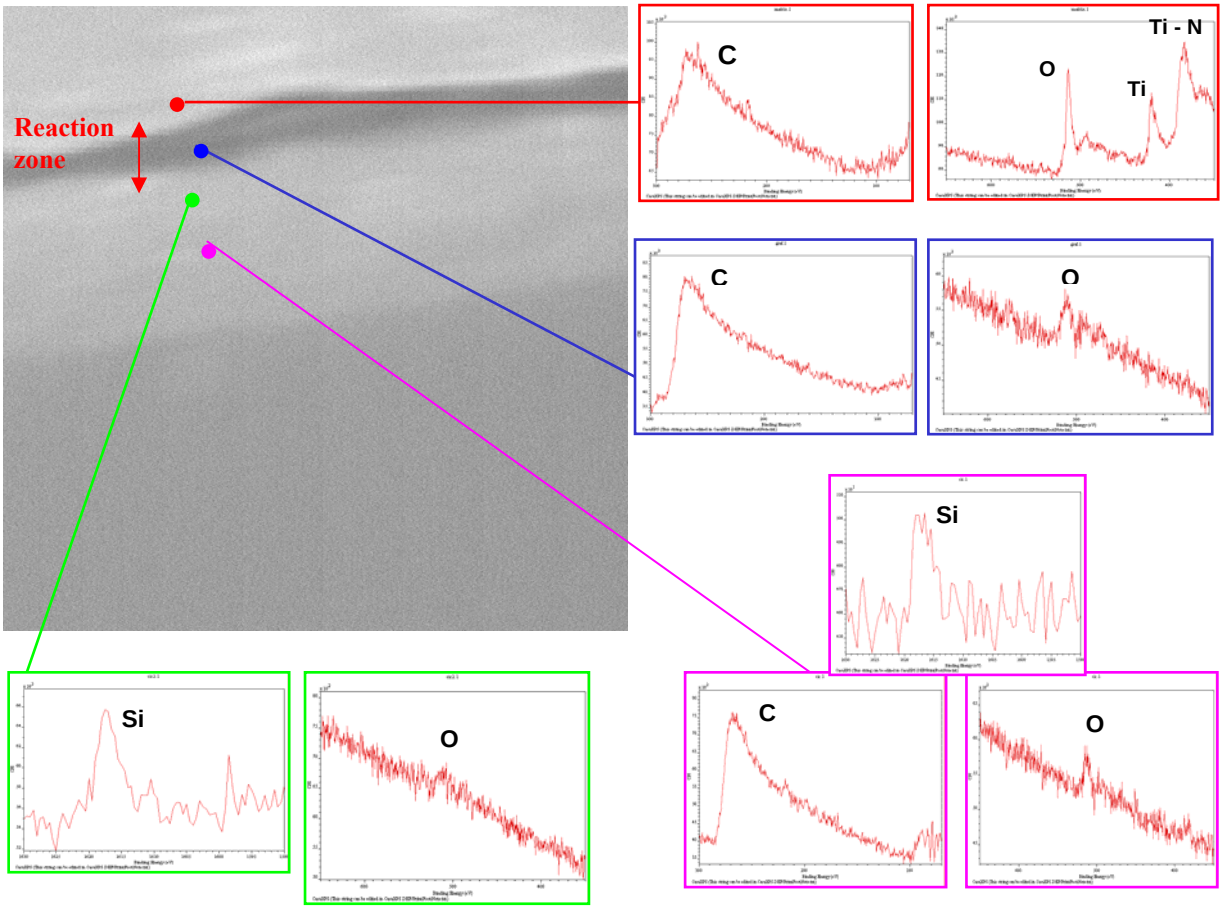

Fig.20 AES observations on the fiber/matrix interface about the treated sample (600°C, 1000 h)

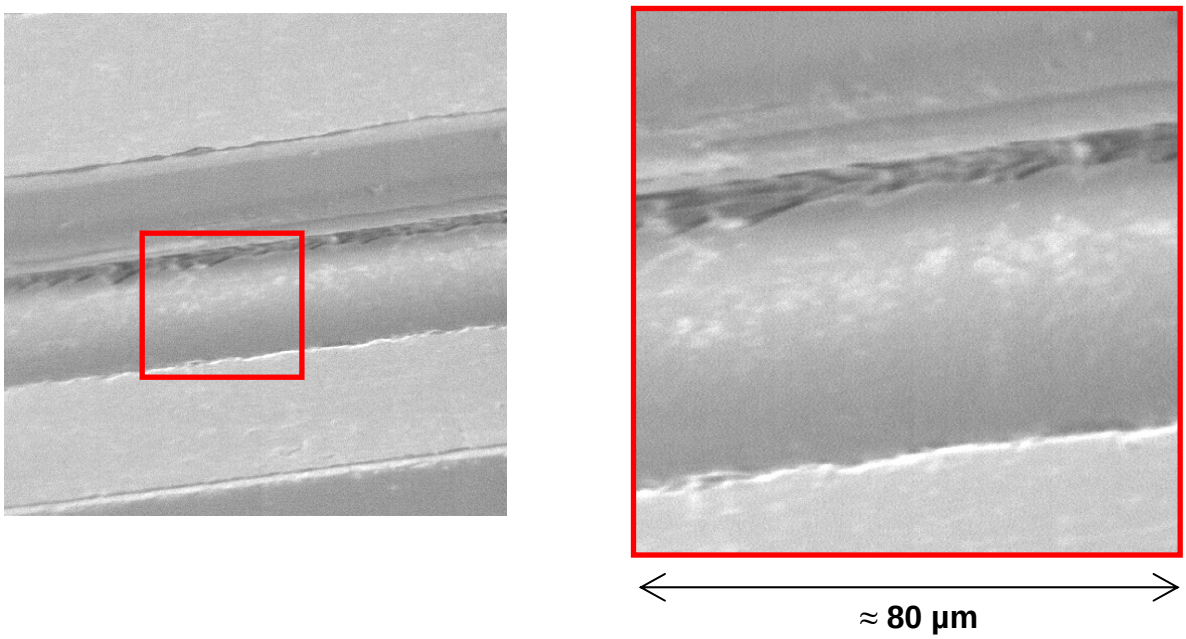

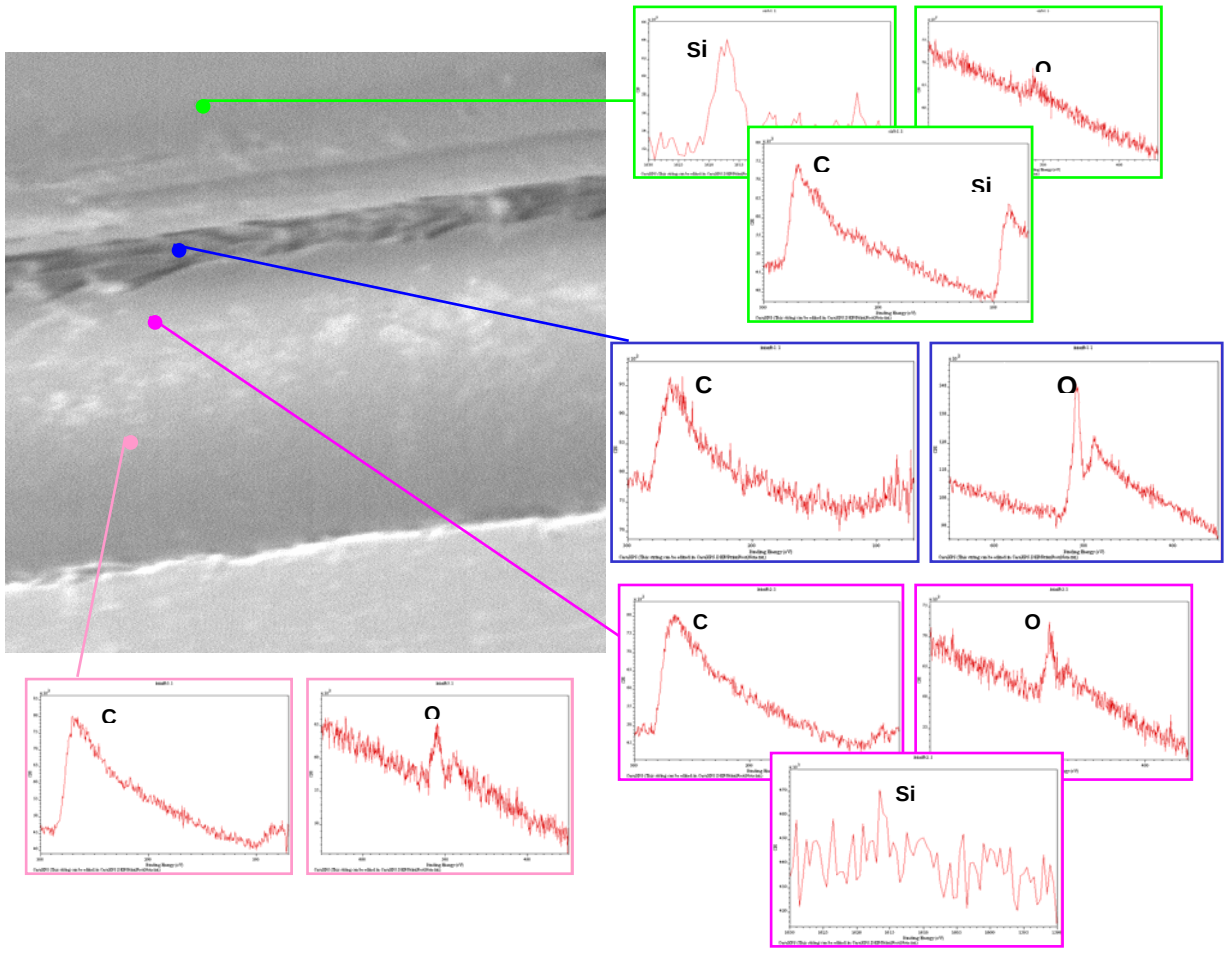

Fig.21 AES observations on the fiber/matrix interface about the treated sample (600°C, 1000 h)

To observe the result repeatability, another zone about the same section on the treated sample (T = 600 °C, t = 1000h) has been selected for the AES measurement (Fig.22).

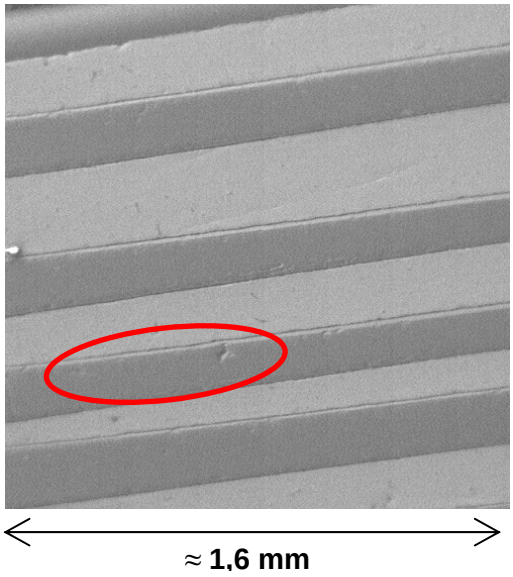

Fig.22 New zone for the analysis of the sample at 600°C and 1000 h

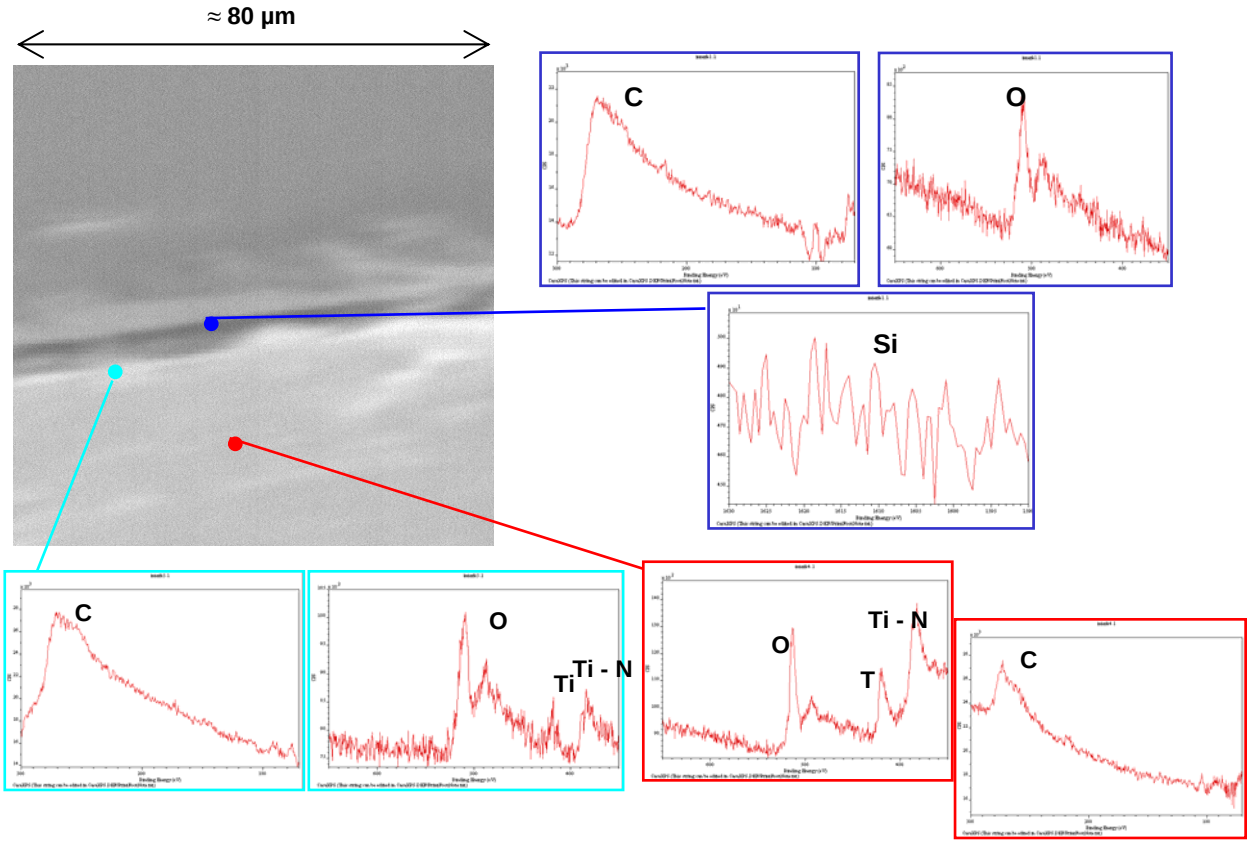

Fig.23 AES observations on the fiber/matrix interface about the treated sample (600°C, 1000 h)

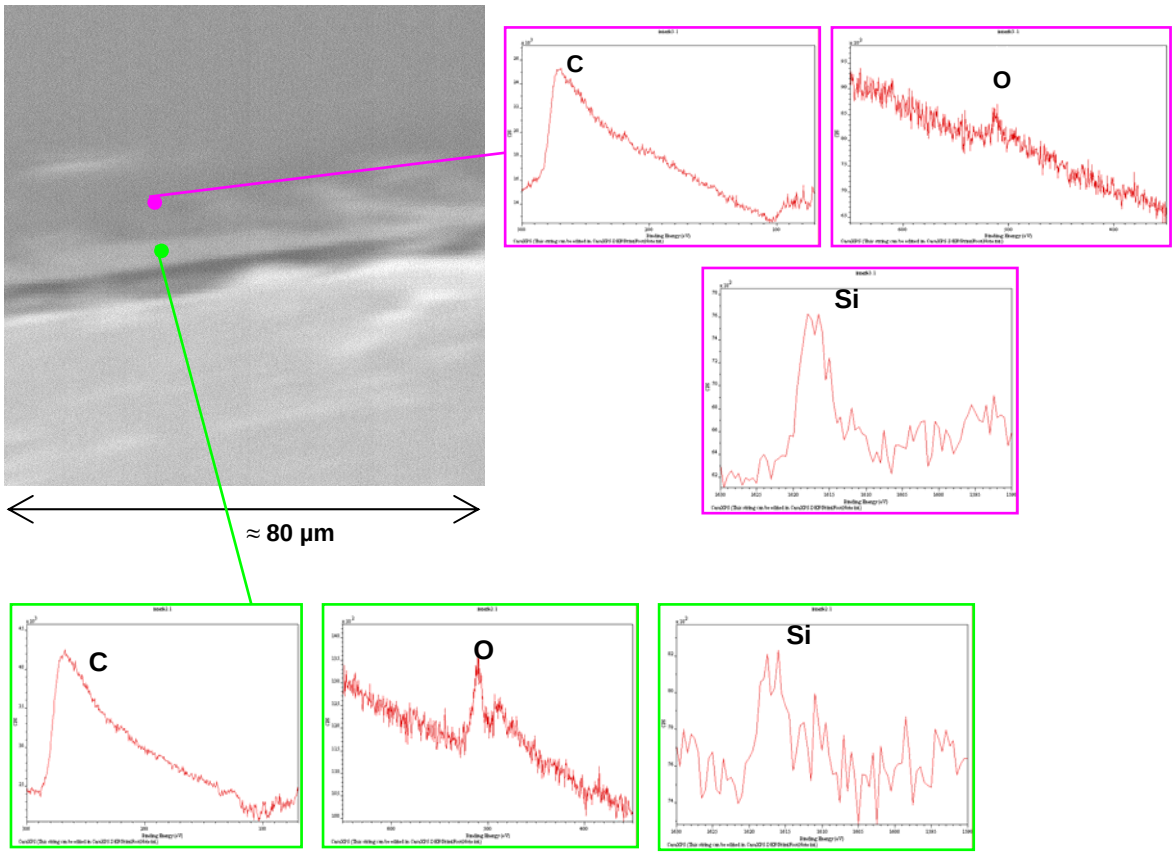

Fig.24 AES observations on the fiber/matrix interface about the treated sample (600°C, 1000 h)

By the direct comparision between the as-fasbricated sample and that heat treated, about the second a higher quantity of oxygen has been noticed. In fact the signal of oxygen is high only at the carbon-matrix interface where titanium is also present.

On the as-fabricated sample a not homogeneous reaction zone is identifiable around carbon coating (Fig.16), about that AES measurement has been carried out. In the heated sample, this reaction zone (Fig.20) is thinner and more uniform than in the as-fabricated one.

Unfortunately, this analysis does not permit to identify directly compounds as the TiC, because the signal of Ti 2p is complex due to the presence of different compounds: nitrides and oxides. In particular, the signals of titanium nitride and titanium carbide are overlapping and the data interpretation is quite difficult.

Other measurements have been developed on the carbon core of the studied fiber (Fig.25).

:

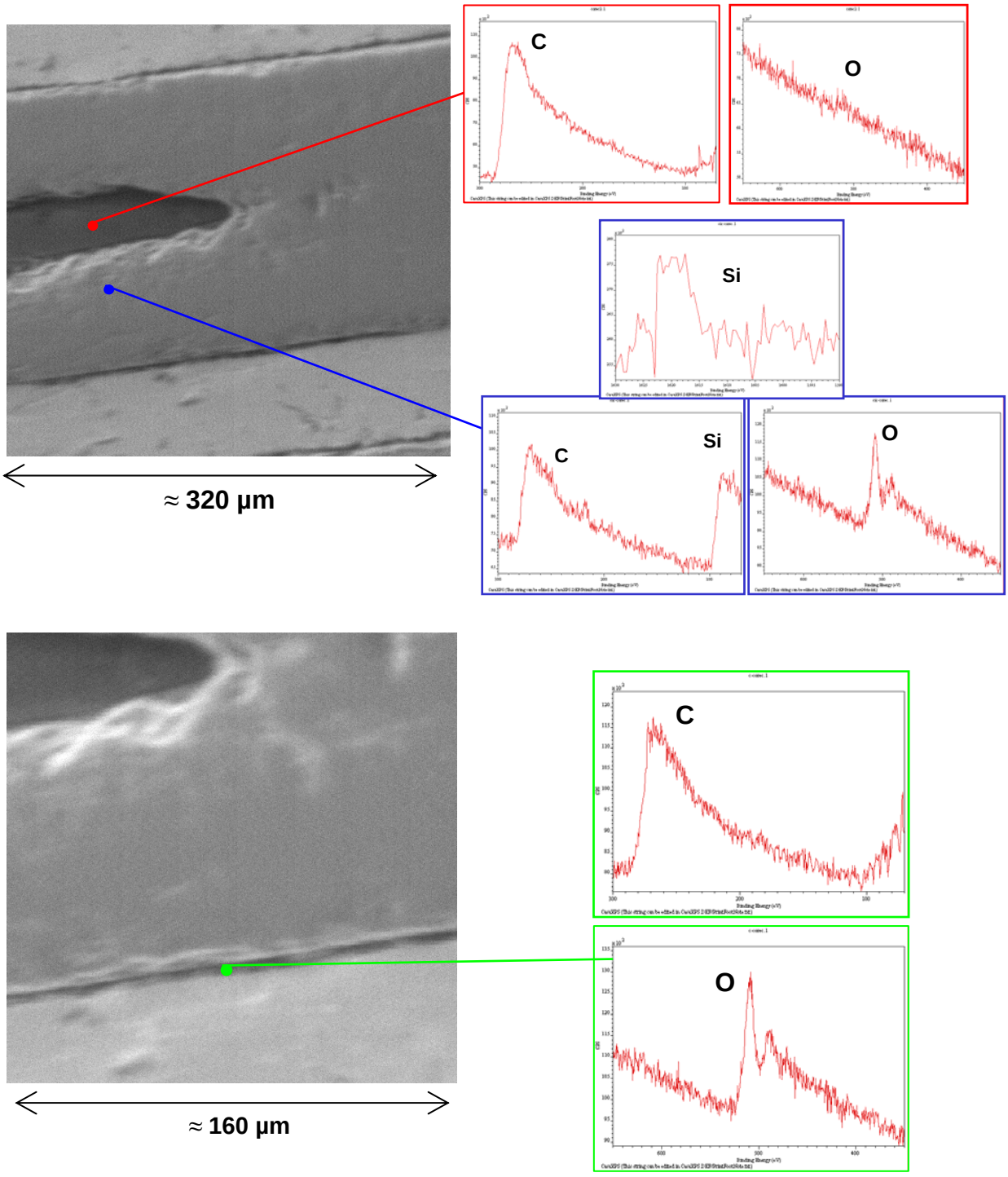

Fig.25 AES measurements on the carbon "core" of the treated sample (600°C, 1000 h)

4.3.2 Zone 2

To get more information, AES measurements have been carried out on the cross-sections of heat-treated samples prepared as described in Fig.9 of Cap.3. In particular the part of the fiber emerging from the matrix has been considered, about the treated sample at 600°C and 1000 hours (Fig.26).

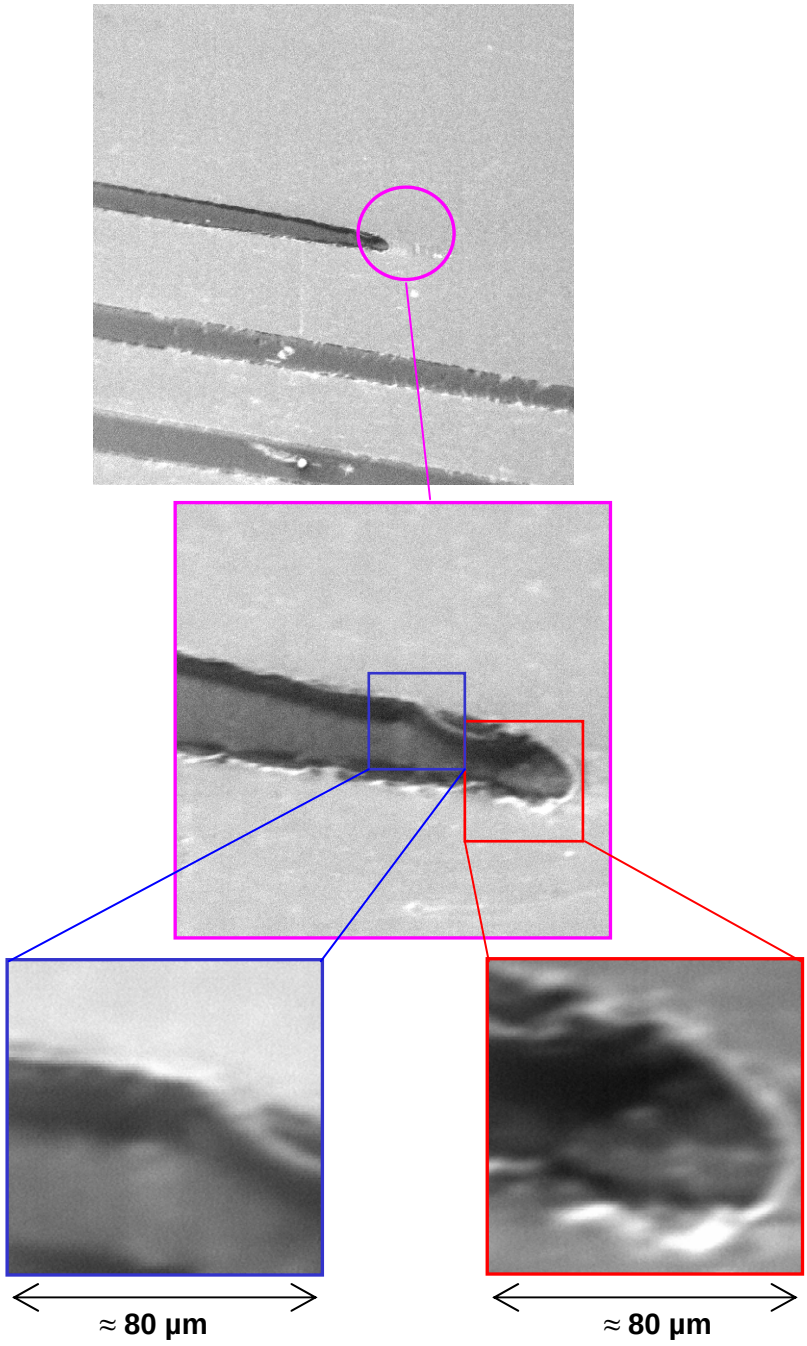

Fig.26 Particular observation zone on the treated sample (600°C, 1000h)

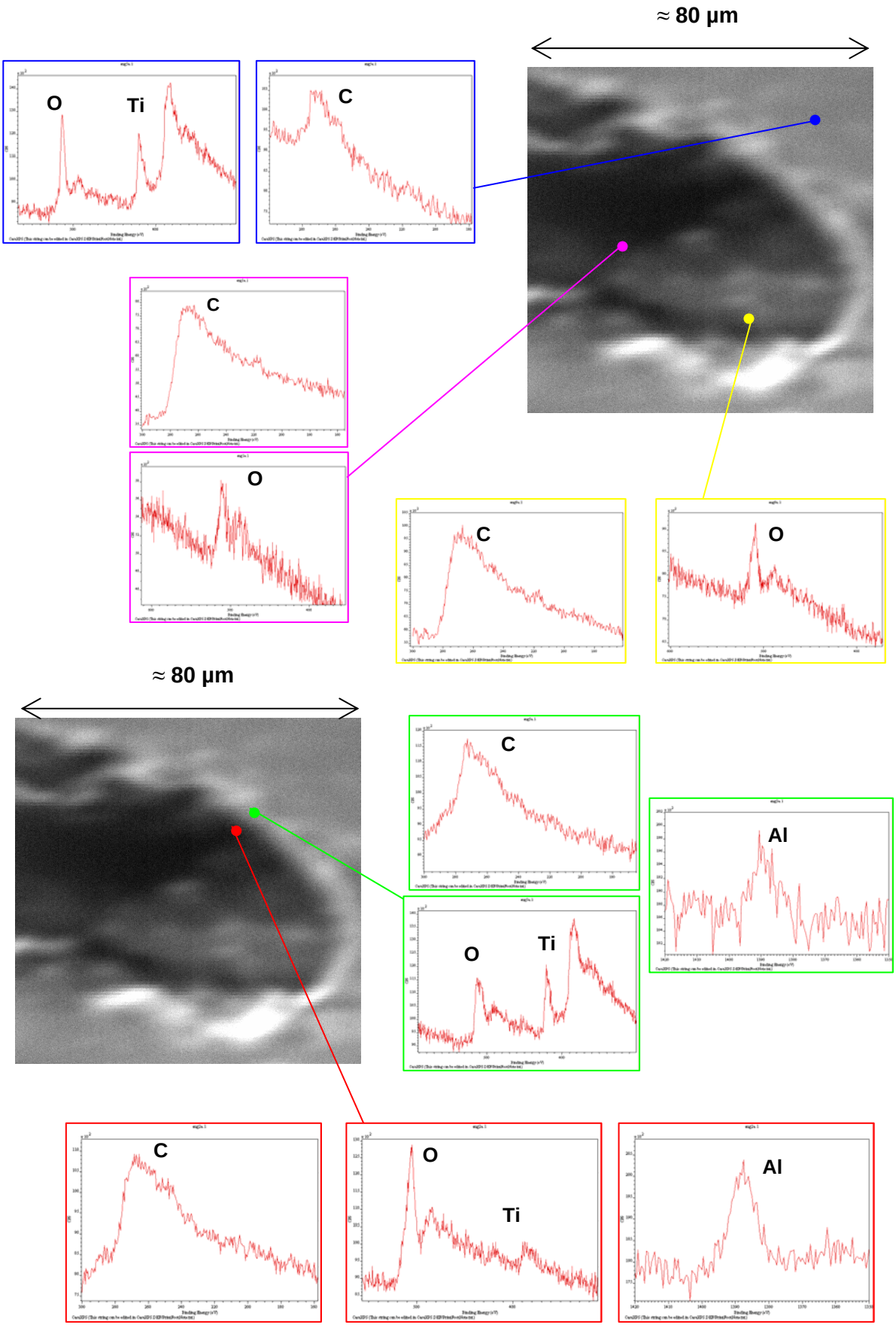

Fig.27 AES observations on sample at 600°C and 1000 h

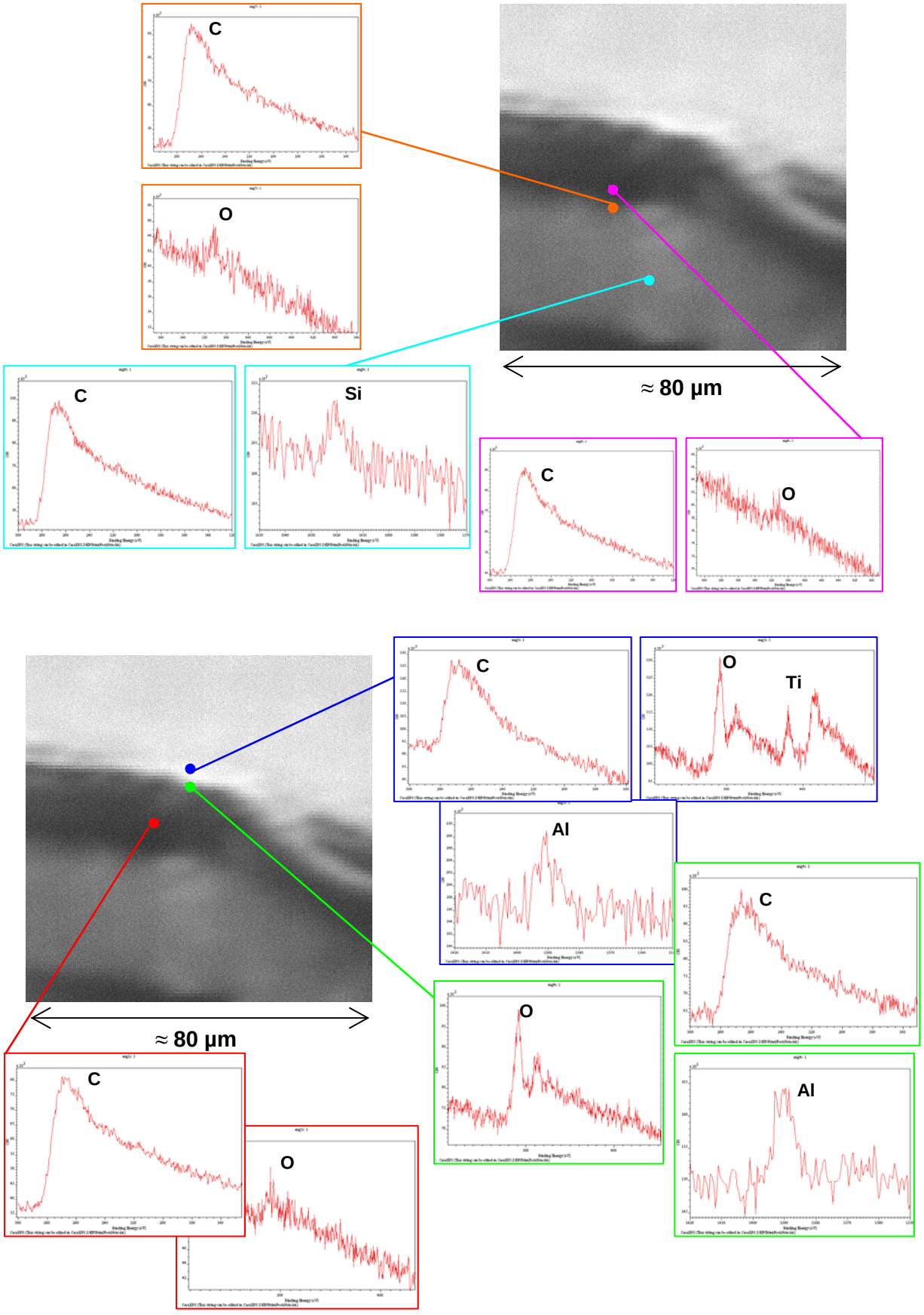

Fig.28 AES observations on sample at 600°C and 1000 h

Fig.27 (upper micrograph) shows carbon inside the matrix, in a position far from the interface. The spectra, recorded in the lower micrograph, evidence titanium traces in the original carbon coating, near to the interface. Therefore, with respect to the as-fabricated condition, carbon is penetrating in titanium and titanium - in carbon. The result is in agreement with experimental facts, observed by other authors [22-24, 31]. The second process (titanium diffusion in carbon) is obviously weaker, because the diffusion of titanium is slower than that of carbon. In fact, there is a zone where both titanium and carbon are present, as shown also by EDS microanalysis.

With the titanium, aluminium has been identified by AES measurements into the carbon coating (Fig.27-28). But probably this datum is due to the mechanical polishing adopted for the sample preparation during that alumina has been used.

4.4 XPS analysis

4.4.1 XPS surface analysis

First of all XPS chemical images, at low resolution, have been carried out to verify the real spatial distribution of the principal elements (Ti, Si and C) of the as-fabricated sample (Fig.29). The same XPS chemical image in Fig.30 (higher magnification), evidence the presence of two different chemical states of carbon: graphite state in the core and coating of fibers (binding energy BE = 284.7 eV) and carbide state in the fiber (BE = 283.0 eV).

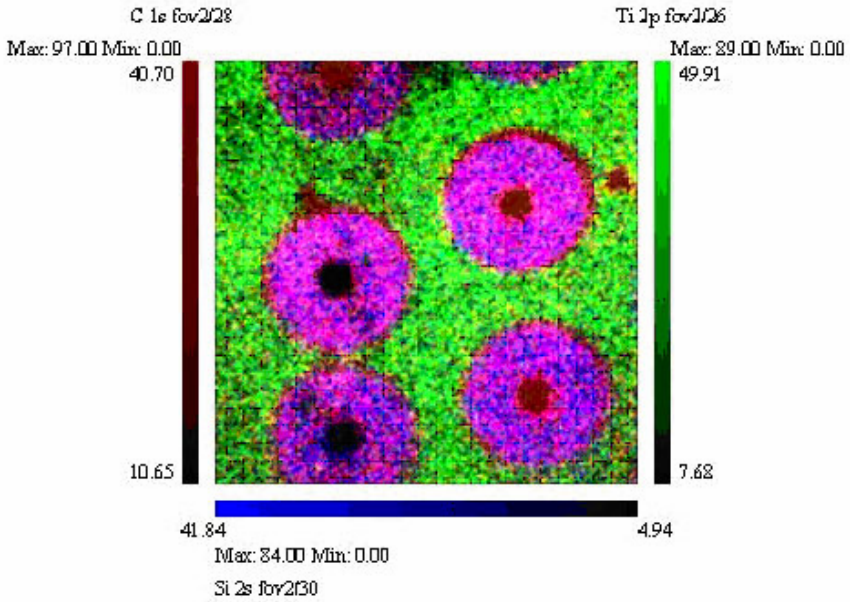

Fig.29 XPS chemical image of Pr1 cross-section: carbon, silicon (Si 2p) in the fiber and titanium (Ti 2p) in the matrix are detected.

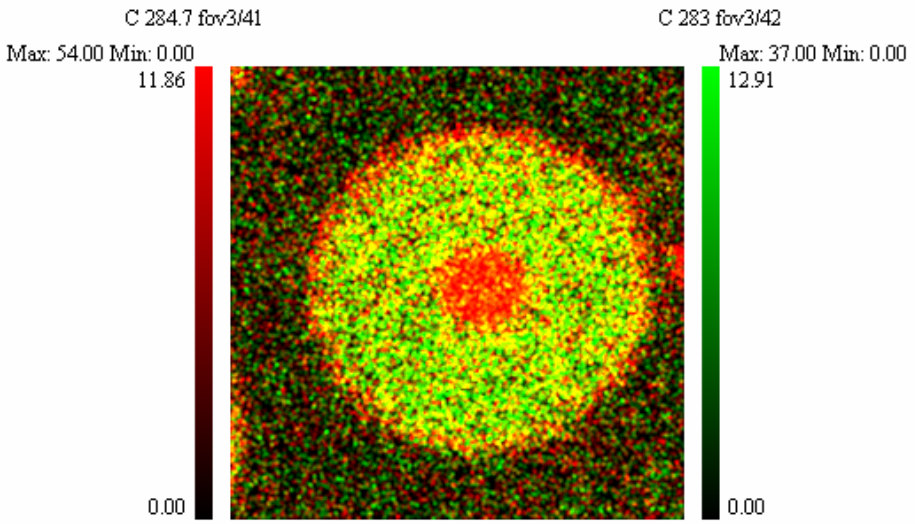

Fig.30 XPS detail: in red carbon-graphite (BE=284.7 eV) on core and coating of the fiber, in green carbon-carbide (BE=283.0 eV) inside the fiber.

The Si 2p signal was characterized by a peak centred at BE = 99.9 eV, that is typical of SiC, and the Si 2p chemical image (not shown) coincided with the carbide image. As it can be seen from this figure, the outer and inner borders of SiC ring confine with graphite. The presence of lower component of C 1s at 284.6 eV in the zone of SiC ring can be explained as carbon contamination.

By the XPS measurements, especially a quantitative analysis has been obtained to value the entity of the aforesaid elements and their chemical composition.

Chemical compositions measured by XPS quantitative analysis on cross sections of 1 mm^2 are reported in Tab.3, where C (carb.) and C (graph.) refer respectively to carbon in form of carbide (SiC) and grafite and C (C=O, C=C) describes the carbon bound with oxygen or in other way with carbon.

Sample	C (carb.)	C (graf.)	C (C=O, C=C)	O	Si	Ti
Pr 1	14.4	15.8	-	14.2	31.3	24.2
Pr 7	11.2	21.7	3.9	21.2	27.4	14.6

Tab.3 Chemical compositions, expressed in at%, of samples as-fabricated (Pr1) and treated at 600°C for 1000 hours (Pr7), obtained by XPS measurements on cross-sections.

The direct comparison confirms that the heat treated material contains more oxygen than the as-fabricated one. In this case the real chemical state of the present oxygen has been possible to estimate too, by the so called “chemical shift” method (Fig.31).

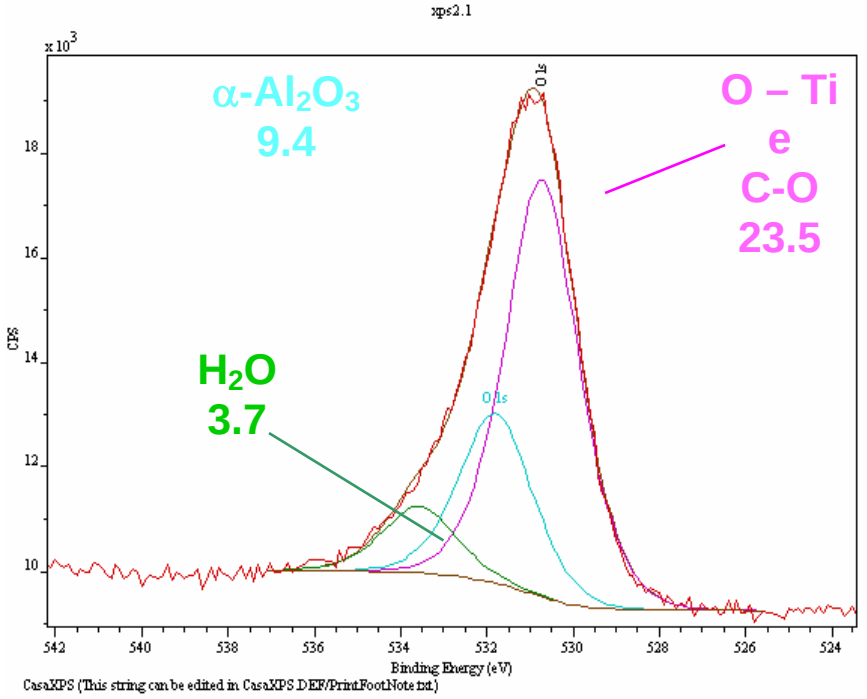

Fig.31 “Chemical shift” about the oxygen XPS spectrum

The result about the XPS quantitative measurements is confirmed by the data on the observation zone , too (Fig.32).

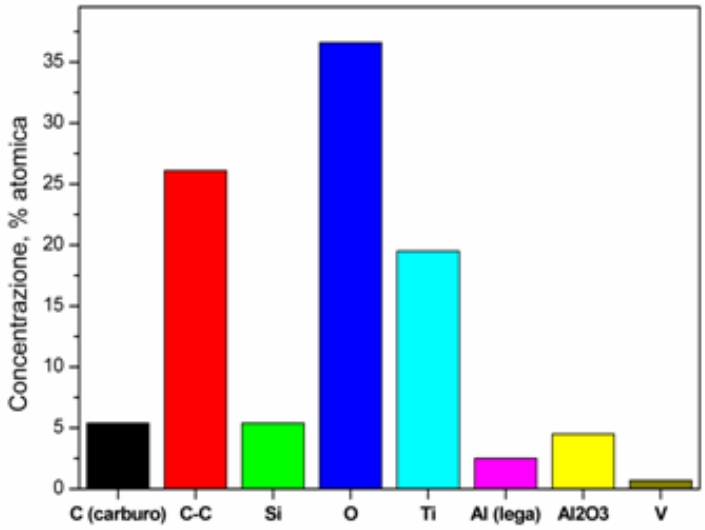

Fig.32 Bar graphic of a quantitative analysis about the found chemical elements

4.4.2 XPS depth profile

As seen about the AES results, but about the XPS measurements too, the considered resolution did not allow to separate the contributions of SiC and other elemt compound as TiC; therefore it was difficult to distinguish a possible formation of TiC at the outer border of the carbon layer. For this reason, the investigation of the interface between carbon and the metallic alloy was continued using Ti6Al4V and Ti99.99+ foils covered with a thin layer of graphite, as described in Fig.11 Cap.3. Especially XPS depth profiles of C-covered samples before and after the heating in vacuum for 8 hours at 500 °C have been recorded and compared.

As it is known, ion sputtering is a destructive process that almost always induces sample modifications. Such a modification occurs in the case of metallic Ti samples where ion sputtering promotes [7] the formation of TiC. In order to reduce the formation of carbide, ion gun was operated at low energy (1.0 keV) and spectra acquisition time was minimized to only 1–2 scans for a region. Nevertheless, the carbides (C 1s at BE = 282.0 eV) have been observed even in the sputtered samples of pure Ti 99.99+ where they were formed from initial surface contamination with carbon (Fig.33). Likewise, carbon contamination is responsible of the formation of carbide species when the pure Ti 99.99+ sample was subject to the thermal process.

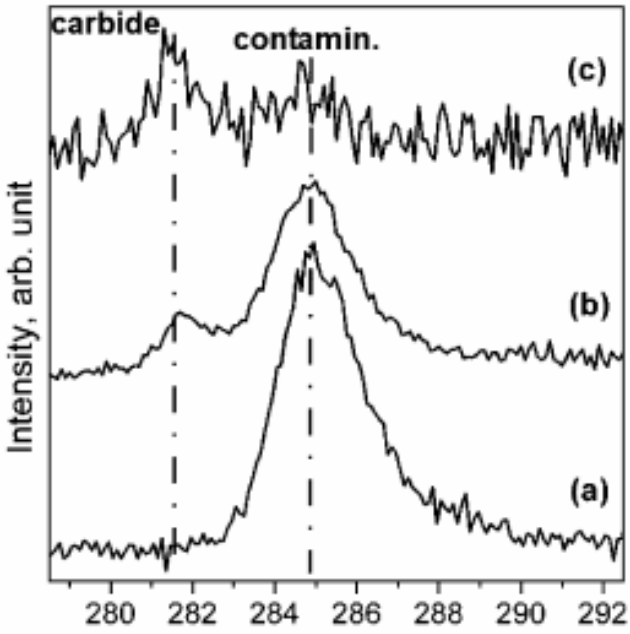

Fig.33 Comparison of C 1s spectra of the: (a) Ti 99.99+ sample as prepared; (b) Ti 99.99+ sample after 30 min of thermal process at 500 ◦C; (c) Ti 99.99+ sample after 140 min of ion sputtering at 1 keV.

Therefore, since the formation of carbides could be caused by thermal process or by ion sputtering, the XPS depth profiles of C-covered samples before and after heating in vacuum for 8 h at 500 °C were acquired and compared.

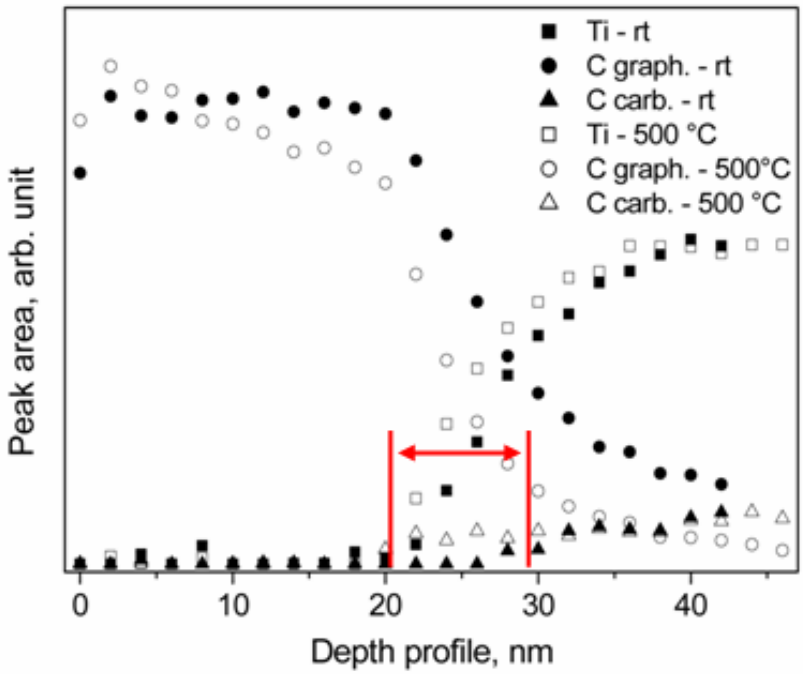

Fig.34 XPS depth profiles of the carbon-covered Ti99.99+ sample at room temperature (r.t.) and after heating at 500 ◦C. The width of the real identified carbide zone of 10 nm is indicated.

Depth profiles were plotted in Fig.34 as peak areas of Ti 2p and C 1s (282.0 eV). After the sample heating, the signal of carbide in the C/matrix interface was increased; moreover, the thickness of the graphite layer was reduced. Considering that the ion sputtering rate was about 0.2 nm/min, the width of the reactive zone due to the thermal process can be estimated to be about 10 nm. Similar results have been obtained from the study of the depth profile of the C-covered Ti6Al4V sample.

4.5 TEM observation

Microchemical aspect about the composite fiber-matrix interface has been studied in depth by T.E.M. observations. In particular by a magnification of 20000x was able to identified the presence of titanium carbide (TiC) around the aforesaid interface (Fig.35).

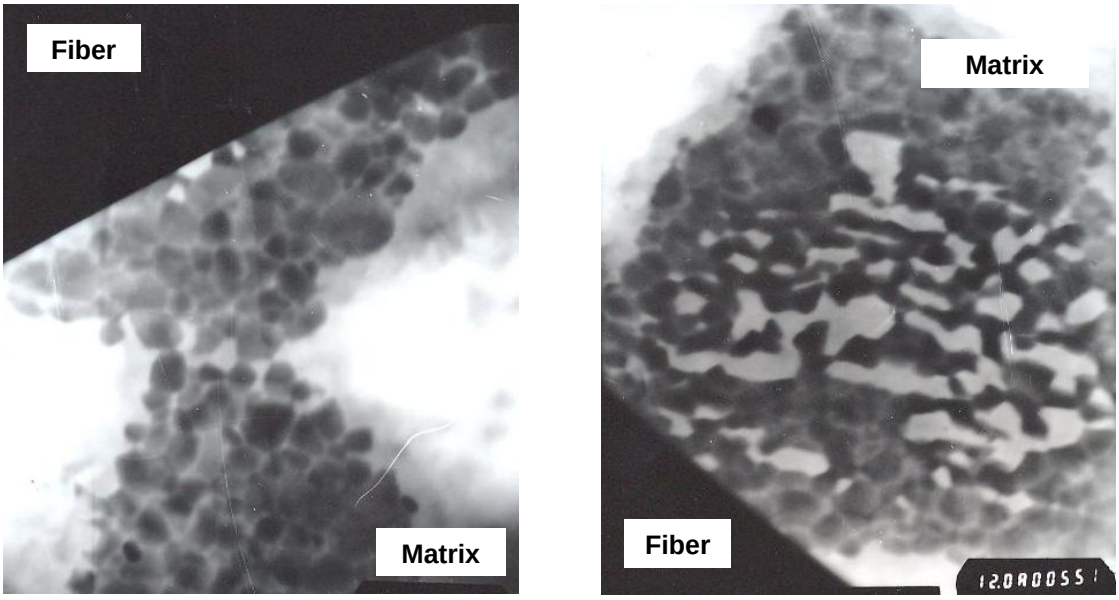

Fig.35 T.E.M. images about the fiber/matrix interface, particular titanium carbide

It's clear by the images in Fig.35 as the formation of the carbide compound is not homogeneous uneven (as realistically expected) but enough to change the diffusion properties of the zone where it forms.

Another interesting aspect by the observations are some "band", identified in the matrix around the fiber (Fig.36). This phenomenon is still under study, especially as regards its chemical, physical or mechanical nature.

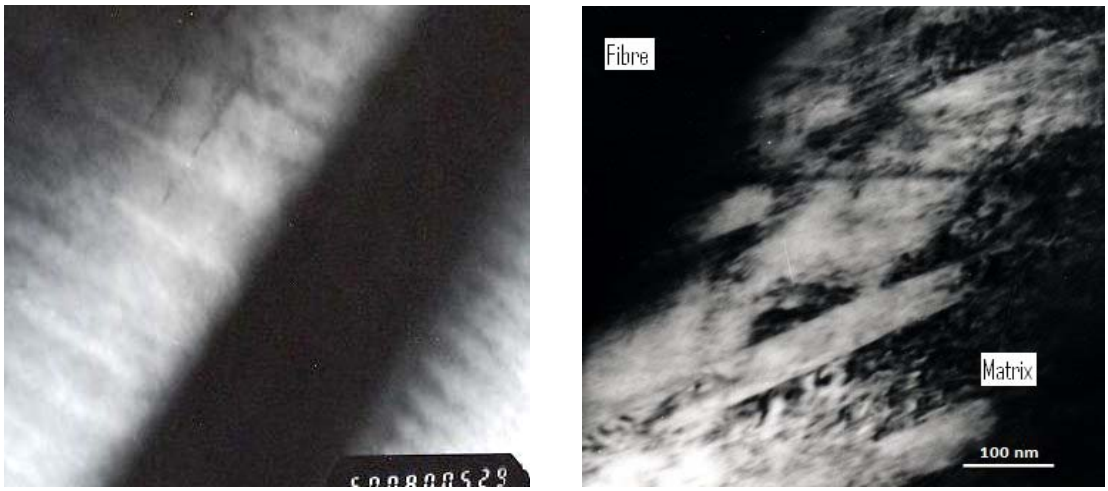

Fig.36 T.E.M. images: particular about the observed band structure

4.6 XRD observation

Both composite and monolithic alloy have been examined by XRD.

From the peak positions of the most intense XRD reflections the interplanar spacings d_{hkl} of composite and monolithic alloy have been determined. For the composite the strain ε_{hkl} on $\{hkl\}$ planes has been calculated by:

$$\varepsilon_{hkl} = \frac{d_{hkl} - d_0}{d_0} \tag{1}$$

where d_0 is the interplanar spacing of the alloy at the same temperature. Fig.37 shows how strain strongly depends on the specific $\{hkl\}$ set of planes. The cell parameters, a and c, of alloy and composite at temperatures up to 600 °C are displayed in Fig.38 (a,b).

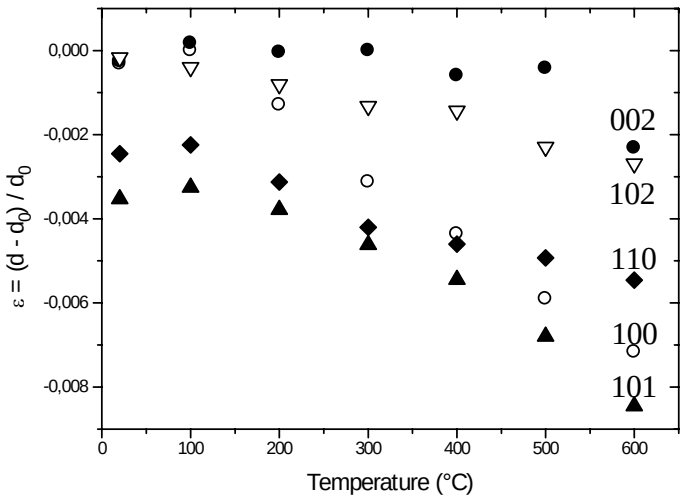

Fig. 37 Strain ε_{hkl} measured by HT-XRD for different {hkl} planes of composite at increasing temperature.

Experimental data can be fitted by the following relationships:

$$a = a_0 (1+\alpha \Delta T) \tag{2}$$

$$c = c_0 (1+\beta \Delta T) \tag{3}$$

where a_0 and c_0 are the cell parameters at room temperature (25°C), α and β the expansion coefficients, ΔT the temperature increase. The values obtained by fitting are reported in Tab.4.

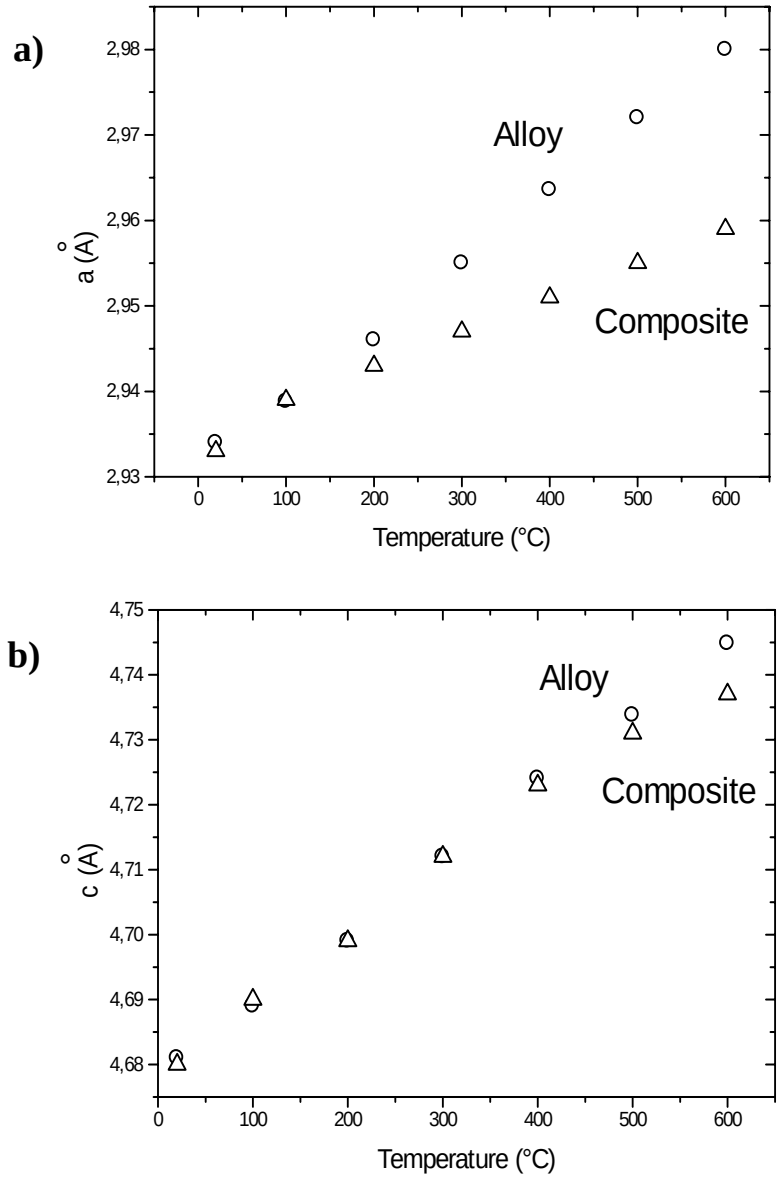

Fig. 38(a-b) Lattice parameters a and c of Ti6Al4V alloy and composite at temperatures up to 600°C.

Material	a_0 **(nm)**	c_0 **(nm)**	α **(°C^{-1})**	β **(°C^{-1})**
Ti6Al4V	0.2934	0.4681	2.32×10^{-5}	2.45×10^{-5}
Composite	0.2933	0.4679	1.36×10^{-5}	2.14×10^{-5}

Tab.4 Ti6Al4V alloy and composite: cell parameters (a_0, c_0) at room temperature and thermal expansion coefficients (α, β).

At room temperature, a_0 and c_0 values of the composite are very close to those of the alloy. When temperature increases both the cell parameters linearly increase but with different rates, namely the h.c.p. unit cell expands modifying its shape. Moreover, the expansion of composite is lower than that of monolithic alloy (Fig.38 a,b) because the fibres, whose thermal expansion coefficient is 4.1 x 10^{-6} °C^{-1}, represent a constraint for the free expansion of the surrounding matrix. Different ε_{hkl} strains on $\{hkl\}$ planes arise from the specific grain orientation with respect the fibres.

Results of analogous experiments performed on the monolithic Ti6Al4V alloy are reported in literature [25-27]. Expansion coefficients determined from tests in vacuum (pressure of 2.5 x 10^{-3} mbar) [25], α = 1.043 x 10^{-5} °C^{-1} and β = 1.448 x 10^{-5} °C^{-1}, are lower than those determined in the present experiments because argon of commercial purity used by us contains residual amounts of oxygen and nitrogen, which are absorbed by the metal during the test in temperature. Cell expansion at high temperature has two components: one is thermal, the other one is due to gas absorption.

The change of a and c in titanium as a function of the amount η of interstitial atoms in the lattice, $da/d\eta$ and $dc/d\eta$ respectively, are 9.0 x $10^{-5}$and 4.0 x 10^{-4} for oxygen, 2.0 x 10^{-4} and 6.7 x 10^{-4} for nitrogen [28], being the values of $da/d\eta$ and $dc/d\eta$ expressed in nm (at %)$^{-1}$. More details about the effects of gas absorption in Ti6Al4V alloy can be found in [29]. Unlike the monolithic alloy, the composite is not free to expand at high temperature due to fibre constraint.

Gas absorption involves a major expansion perpendicularly to $\{002\}$ planes because $dc/d\eta > da/d\eta$ thus the grains with [002] direction parallel to the fibre axis are more affected by constraining than those with [002] direction perpendicular. So, taking also in consideration the different values of α and β of composite and alloy, it seems reasonable to conclude that gas is preferentially absorbed by those grains with a favourable orientation with respect the fibres ([002] perpendicular to major fiber axis).

Peak profiles of the alloy are quite broader than those of the composite.

Fig.39 displays the $\{100\}$ reflections whose intensities have been normalized for making easier the comparison.

For each XRD reflection the total line broadening β_T , corrected from instrumental broadening, is basically due to two contributions, the size of coherently diffracting domains (β_D) and the micro-strains (β_ε). β_T can be written as the (4):

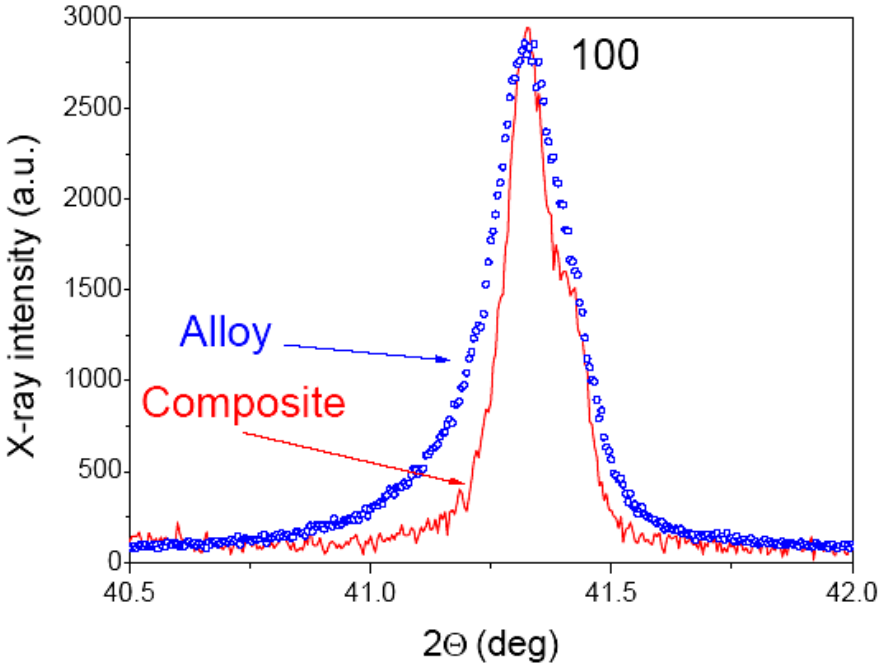

Fig.39 Precision {100} XRD peak profiles of alloy and composite.

$$\beta_T = \beta_D + \beta_\varepsilon = \frac{K\lambda}{D\cos\vartheta} + 2\varepsilon\tan\vartheta \qquad (4)$$

where D is the domain size, ε the average micro-strain, ϑ the Bragg angle, λ the X-ray wavelength and K a constant (= 0.89). In the case of Ti and Ti alloys the coherently diffracting domains are the grains which from metallographic observations result to be near of the same mean size ($D \approx 30$ μm) in alloy and composite. Being the grain size very large, the β_D term in eq. (4) can be neglected:

$$\beta_T \cong \beta_\varepsilon = 2\varepsilon\tan\vartheta \qquad (5)$$

Introducing the β_T values of the main XRD reflections into eq. (5), the micro-strain ε has been determined. Finally, the dislocation density ρ was calculated by means of the Williamson-Smallman relationship [30]:

$$\rho = \Xi\,\varepsilon^2 / k_0\, b^2 \qquad (6)$$

where Ξ =16 is a constant, b is the modulus of Burgers vector and $k_0 \cong 1$ is a factor depending on dislocation interaction. From this calculation the values of $\rho = 6.1 \times 10^9$ cm^{-2} for the composite and $\rho = 5.5 \times 10^{10}$ cm^{-2} for the monolithic alloy have been obtained.

4.7 Internal Friction

To observe in the better way the suitability of the studied material during the work condition, an analysis about the fiber/matrix interface has been carried out by a by dynamic point of view. About that, the composite has been investigated by internal friction (IF) measurements in the temperature range 300-1173 K, followed by a cooling time to verify the reversibility of the observed phenomena (Fig.40). Every measurement has been developed by different resonance frequency.

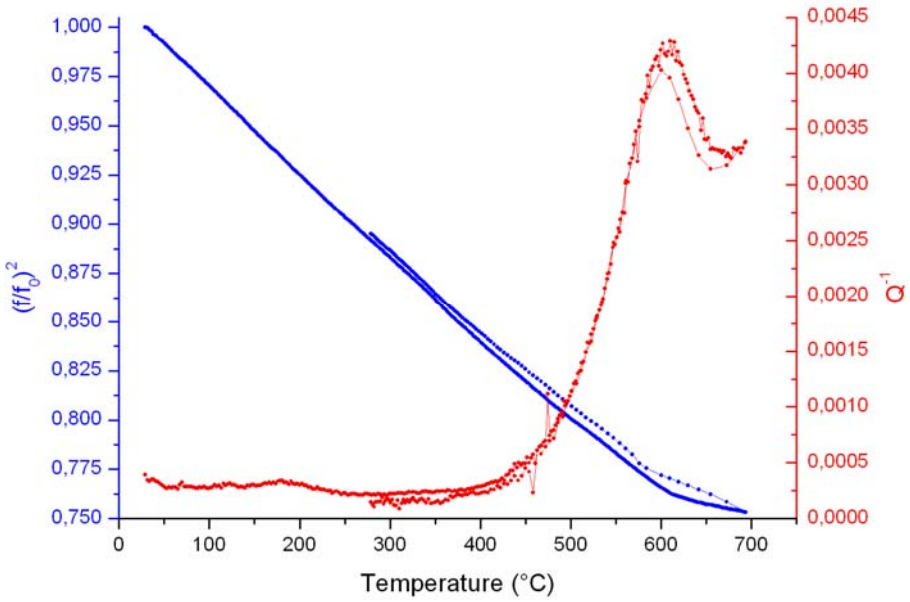

Fig.40 Internal friction Q^{-1} and elastic modulus $(f/f_0)^2$ for the Ti6Al4V-SiC$_f$ composite, included the cooling phase

Fig.30 and Fig.32 shows Q^{-1} and $(f/f_0)^2$ vs. T trends of the composite. The Q^{-1} curve shows a peak at about 873 K. superimposed to an exponentially increasing background, in correspondence of the peak the modulus exhibits a change.

Repeated tests on the same sample do not induce permanent changes of resonance frequency f_0 and Q^{-1} at room temperature. After heat treatments of 1.8 x 10^4 s at 1073 K the IF peak is still present without remarkable intensity variation.

For comparison the monolithic Ti6Al4V alloy has been submitted to the same experiments (Fig.41-42). In this case the alloy doesn't show the IF peak but only the exponential background, higher than that of composite.

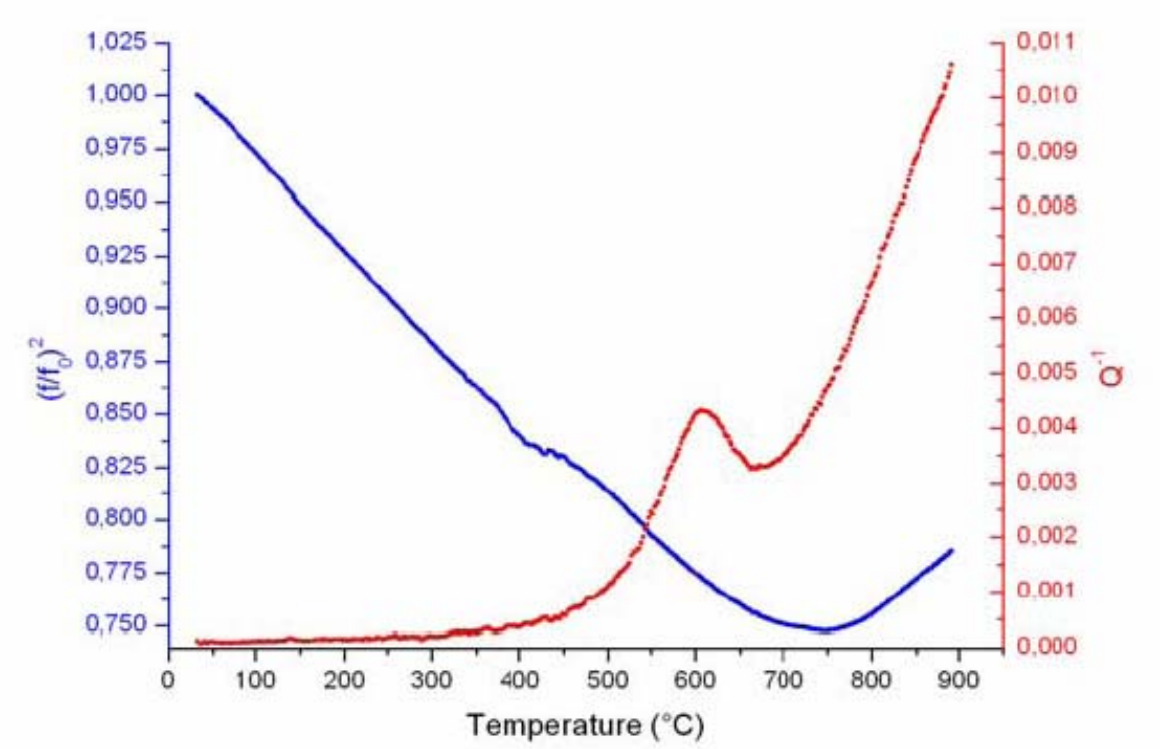

Fig.41 Internal friction Q^{-1} and elastic modulus $(f/f_0)^2$ for the Ti6Al4V-SiC$_f$ composite

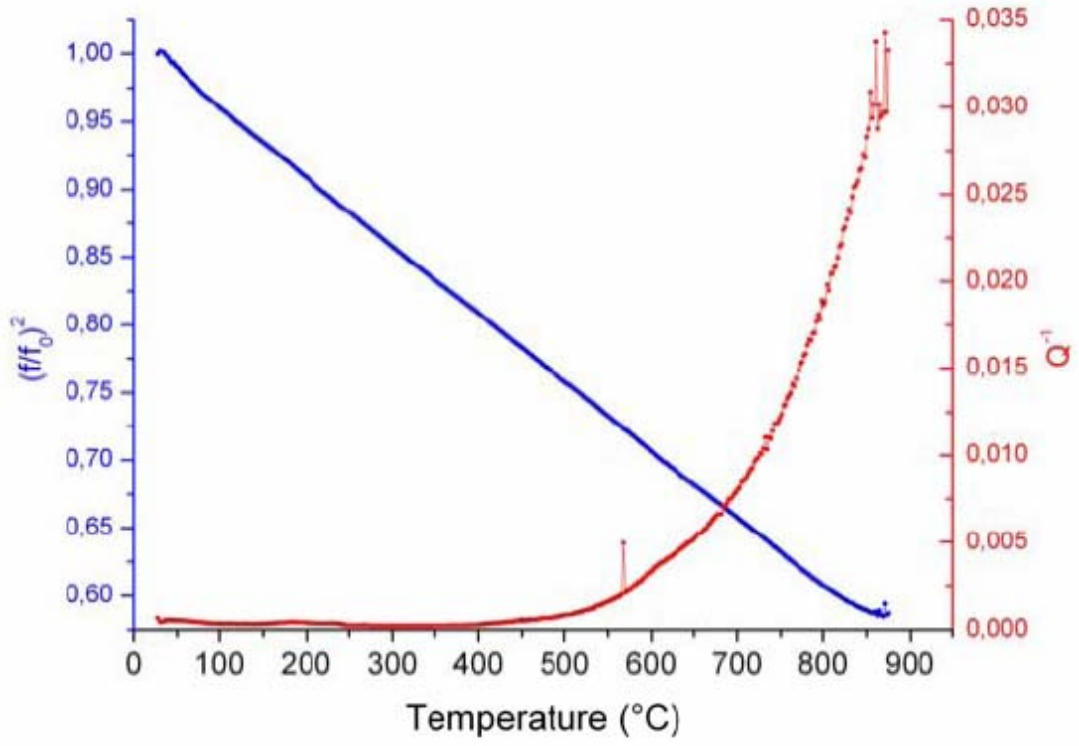

Fig.42 Internal friction Q^{-1} and elastic modulus $(f/f_0)^2$ for the Ti6Al4V alloy

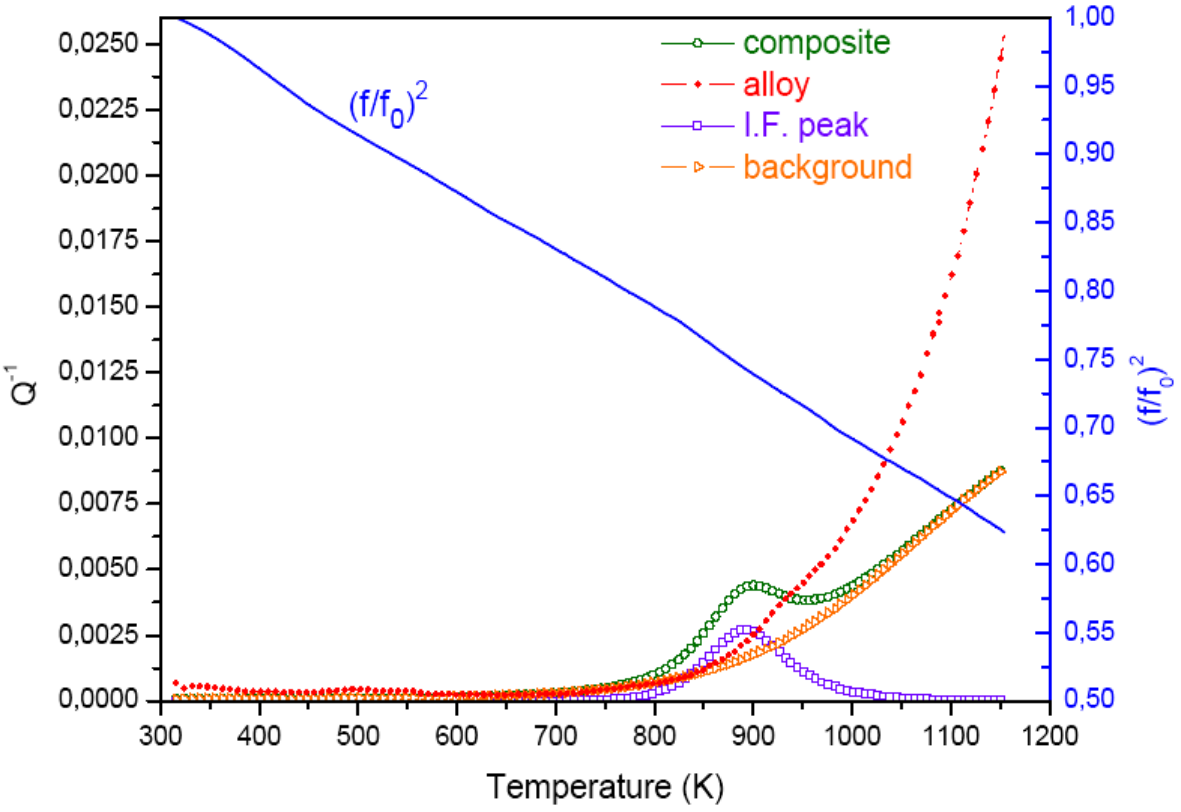

Fig.43 Background interpolation and resulted peak for the Q^{-1} vs. T trends of the composite and the Ti6Al4V alloy

As showed in Fig.43, it has been useful to proceed with a "fitting" operation of the obtained relaxation peak (resulted by the difference between the experimental trend and the interpolated background) by a note equation. In particular it was possible to verify as the peak is may be interpolated very well by a Debye peak, many times used about the internal friction theories to describe typical peaks. The Debye peak is described by the formula:

$$Q^{-1} = \Delta \sec h\left[\frac{H}{R}\left(\frac{1}{T} - \frac{1}{T^*}\right)\right] \tag{3}$$

where Δ is the peak height, R gas constant, T^* maximum temperature for the peak, H the activation energy. This energy has been calculated as first approximation, by the experimetal data of the first two probes, by the following formula (4)

$$\Delta H = R \cdot \left[\frac{\ln\left(\frac{\omega_2}{\omega_1}\right)}{\frac{1}{T_1} - \frac{1}{T_2}} \right] \tag{4}$$

with T_1 e T_2 peak temperature and ω_1, ω_2 the corresponding resonance pulsation.

According to these considerations the right fitting has been developed for each measurement (Fig.44).

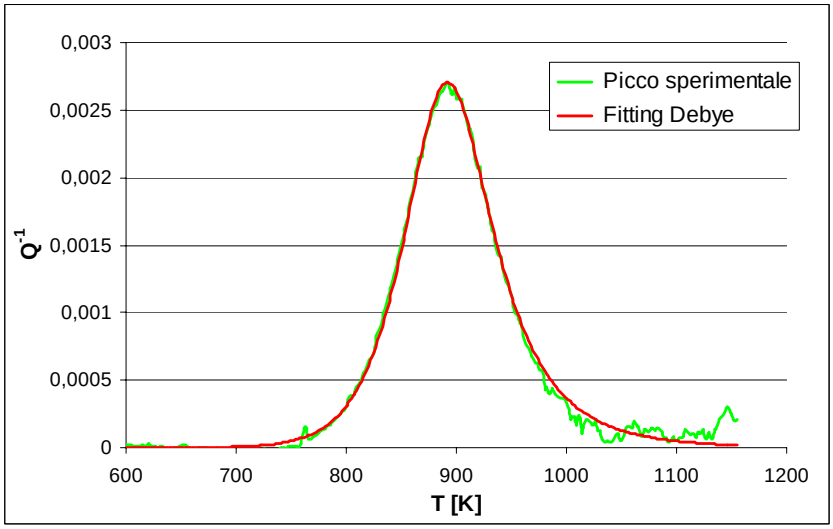

Fig.44 Fitting of experimental peak by Debye peak

By Fig.45, it's possible to verify as the peak position depends on the frequency, according the formula (4).

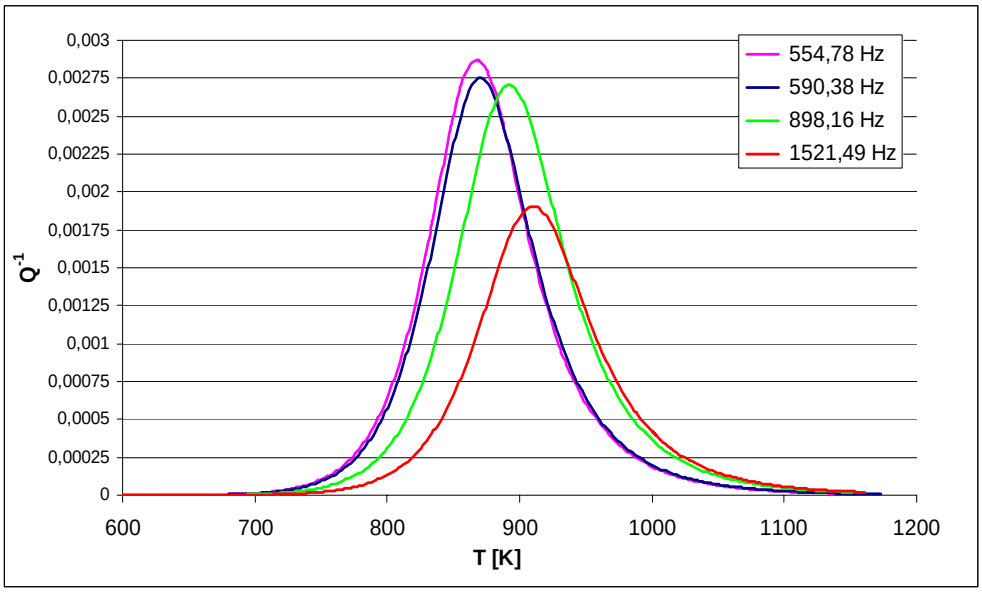

Fig.45 Comparison between relaxation peak at different resonance

Other important parameters to define the observed relaxation process are certainly relaxation time τ, distintive for each tests, and the relaxation time constant τ_0. The latter constant , independent by temperature, has been calculated about $2{,}3*10^{-15}$ s.

Both parameters are so obtainable:

$$\omega \cdot \tau = 1$$
$$\tau = \tau_0 \cdot e^{\frac{\Delta H}{R \cdot T}} \quad (5)$$

By this way all characteristic parameters of the relaxation process have been obtained for each experimental trend. (Tab.5).

	T [K]	Q^{-1}	f [Hz]	ω [Hz]	τ [s]
Pr.3	876,8525	0,002751	590,3861	3709,505	2,696E-04
Pr.5	891,9861	0,002706	898,1653	5643,339	1,772E-04
Pr.9	910,1154	0,001992	1521,496	9559,843	1,046E-04
Pr.10	873,9504	0,00287	554,7822	3485,800	2,871E-04

Tab.5 Obtained parameters about the IF measurements at high temperature

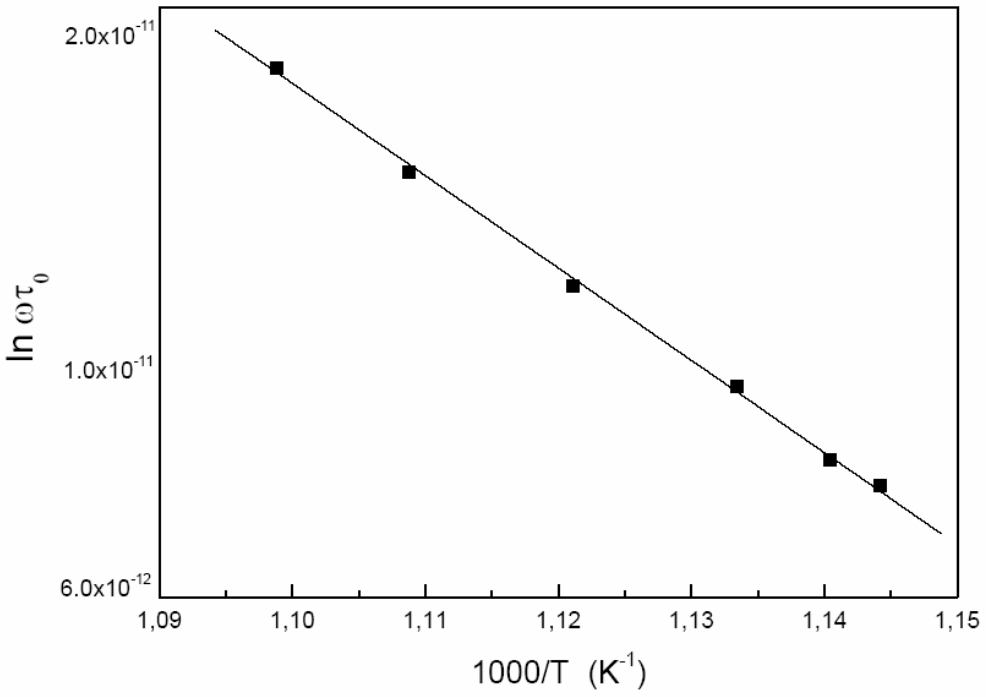

Fig.46 Arrhenius plot by the carried experimentation (activation energy H = 186 kJ/mole and the relaxation time $\tau_0 = 2{,}3 \times 10^{-15}$ s have been obtained)

Having more probes, an Arrhenius plot can be draw, as showed in Fig.46. In this case the angular coefficient of the line that interpolates the experimental points is the real activation energy *H*. The characteristic value results 185,5 kJ/mole, very close to typical values of activation energy for diffusion phenomena.

As previously disclosed, the experimentation about the difference between the considered composite realized by the two different fabrication process has been developed and an important part has regarded the IF studies, by measurements carried out by the same aforesaid concepts. In particular Fig.47 shows the IF trend vs temperature, for the composite produced by *Roll Diffusion Bonding*.

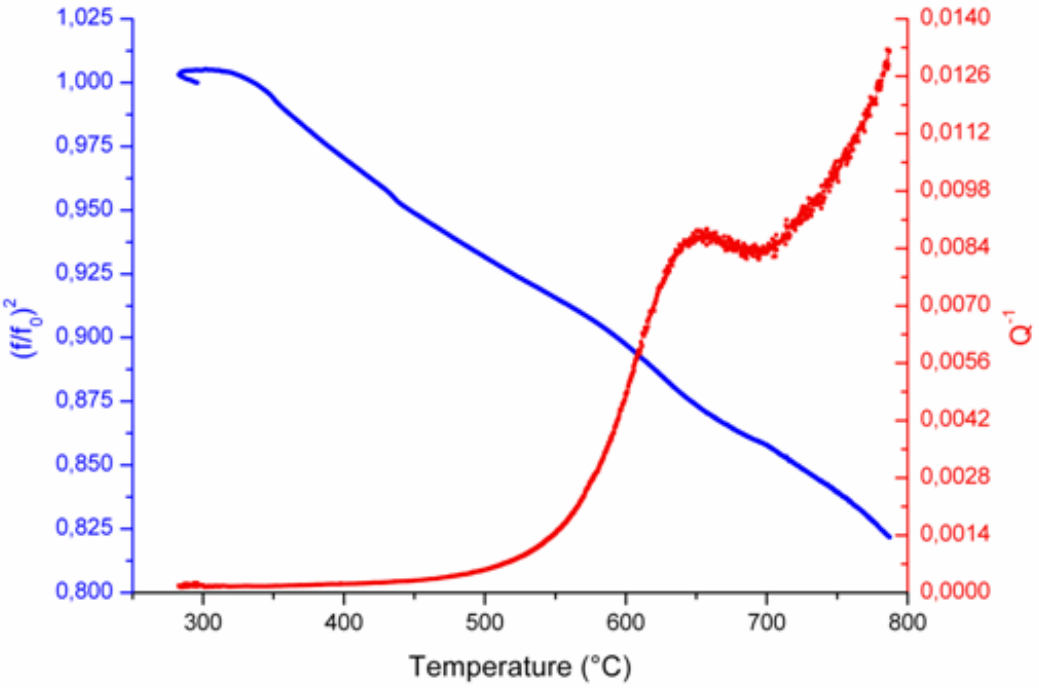

Fig.47 Internal friction Q^{-1} and elastic modulus $(f/f_0)^2$ for the Ti6Al4V-SiCf composite produced by Roll Diffusion Bonding

About that it is possible to note also in this case the presence of a relaxation peak at about 600°C, added to a background of exponential type. By the fitting data carried already for the HIP composite, the Debye peak has been found for the RDB composite, too. In particular by the eq.(4), the activation energy of this case has been calculated: 189 kJ/mole.

In particular Fig. 49 shows the comparison between the tests for the two typologies of composite, carried out at the same frequency condition.

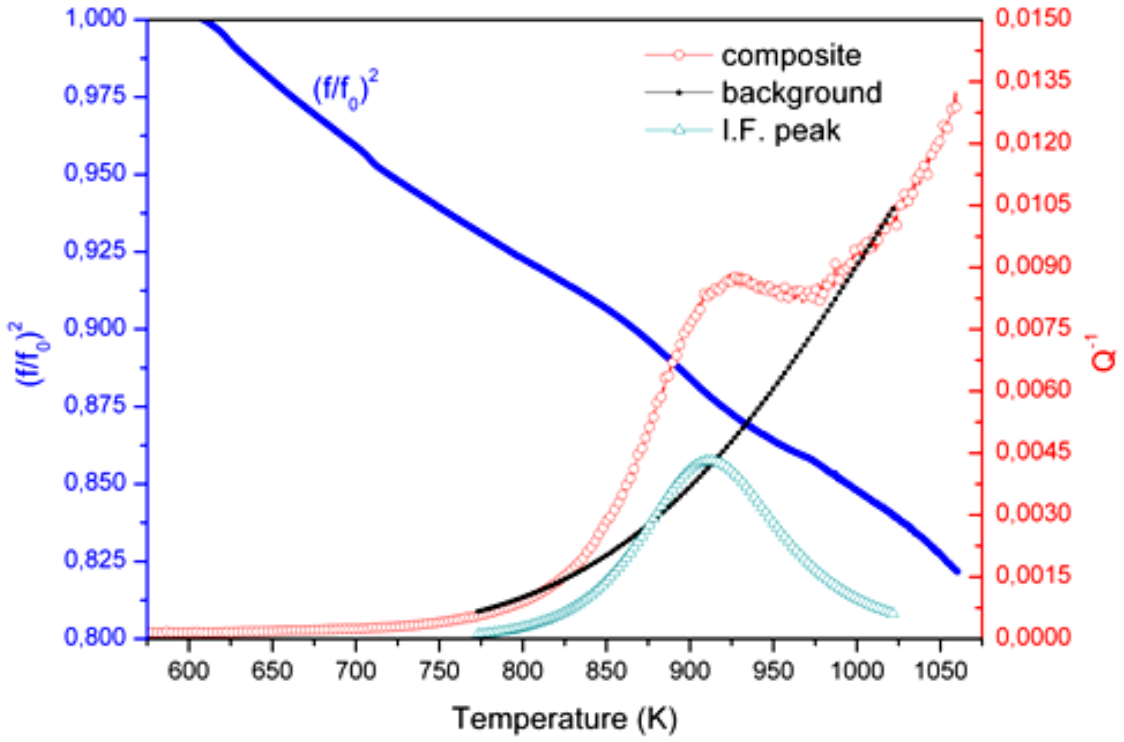

Fig.48 Background interpolation and resulted peak for the Q^{-1} vs. T trends of the R.D.B. composite

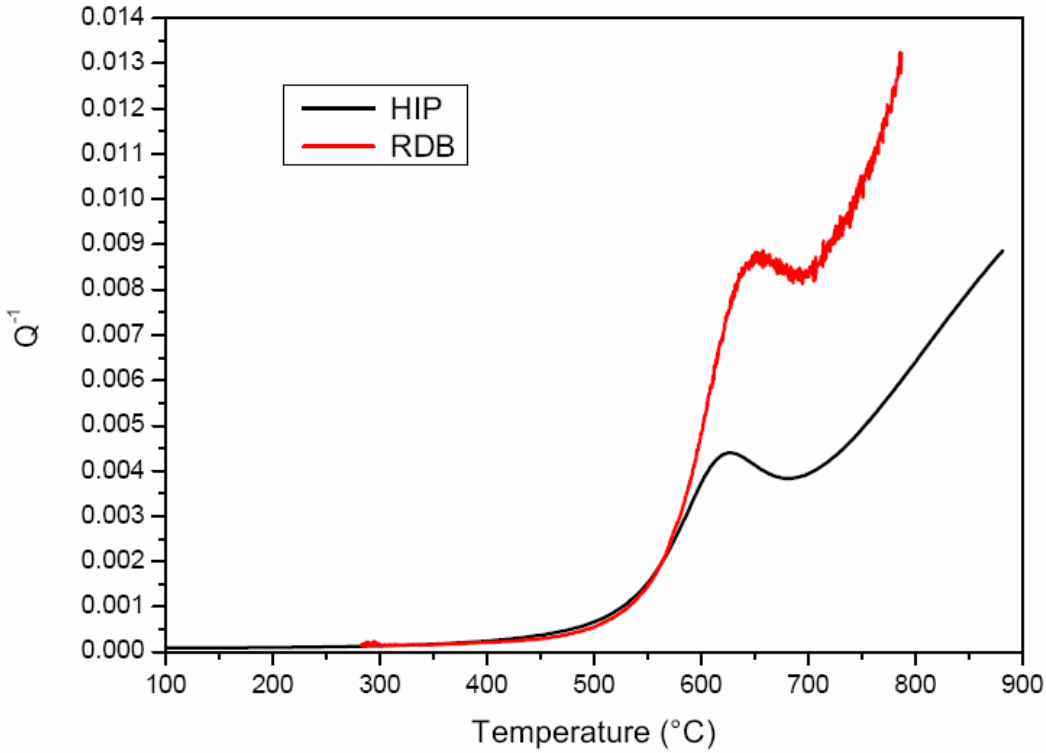

Fig.49 Comparison between Internal Friction probes for HIP composite and Roll Diffusion Bonding composite

4.8 Discussion

Micro-chemical analyses (EDS, AES and XPS) do not show remarkable changes of carbon-matrix interface after the heat treatments considered here; the result is in good agreement with those of mechanical tests carried out on samples in the same conditions (see Cap.5).

To understand the high structural stability of the material, the growth of reaction zone for the conditions of material production and heat treatment has been calculated. Its thickness x vs. time t is expressed by [31]:

$$x = kt^{1/2} \tag{1}$$

$$k = k_0 e^{-\frac{Q}{2RT}} \tag{2}$$

being T the treatment temperature, Q the activation energy, k_0 the pre-exponential factor and R the gas constant. The values Q = 252 kJ/mole and k_0 = 4.88 x 10^{-3} $ms^{-1/2}$ introduced in eq. (2) are those determined by Gundel &. Wawner [31] for a (α+β) structure.

The thickness calculated for fabrication condition (T_1 = 890 °C, t_1 = 1,5 hours) is 0,78 μm while for heat treatment condition (T_2 = 600°C, t_2 = 1000 hours) is 0,26 μm. In spite of overestimation, the reaction zone due to heat treatment is thinner than that due to fabrication process.

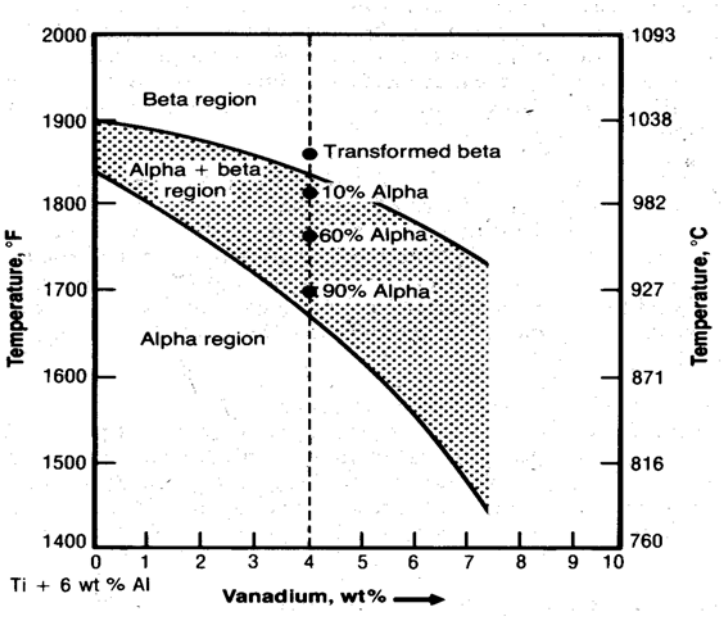

Fig.50 Particular of the Ti6Al4V phase diagram

In fact since carbon diffusion is larger in β than in α phase of Ti6Al4V alloy, the calculated value *x* of heat treated sample will overestimate the real one because at 600 °C the matrix is made exclusively of α phase (Fig.50). Moreover, the heat treated material already has a zone of reaction, formed during fabrication process, thus carbon moves first through the TiC layer (slower diffusion), then through the matrix (faster diffusion).

Another very important comparison between experimental data and diffusion theories is useful to verify the presence and the influence of aforesaid titanium carbide on the fiber-matrix interface. In fact the experimental XPS depth profiles (developed and showed as in Fig.11, Cap.3) can be compared with carbon concentration profiles calculated by the 2nd Fick's law in the case of a semi-infinite solid. It is given by:

$$\frac{C_s - C_x}{C_s - C_0} = erf\left(\frac{x}{2\sqrt{Dt}}\right) \tag{3}$$

where *C*s is the carbon concentration at the surface (100%), C_0 is the carbon concentration in the solid far from the surface (0%), C_x is the carbon concentration at a depth *x* after the exposure time *t* at the temperature *T*. The term *D* is the diffusion coefficient of the carbon in the solid given by:

$$D = D_0 e^{-\frac{Q}{RT}} \tag{4}$$

Where D_0 is a constant pre-exponential factor and *Q* is the activation energy. The carbon concentration profile calculated for the diffusion of carbon in Ti-*α* after 8 h (2.88×104 s) at 500 ◦C is showed in Fig.51. The values of D_0 and *Q*, taken from Ref. [32], are displayed in Fig.40, too. It is clearly shown that carbon diffuses over a distance of about 10 μm. The calculated value is three orders of magnitude higher than the experimental value of 10 nm (obtained by the XPS profile); thus carbon concentration in the interface cannot be explained by the process of carbon diffusion in the Ti-*α* matrix.

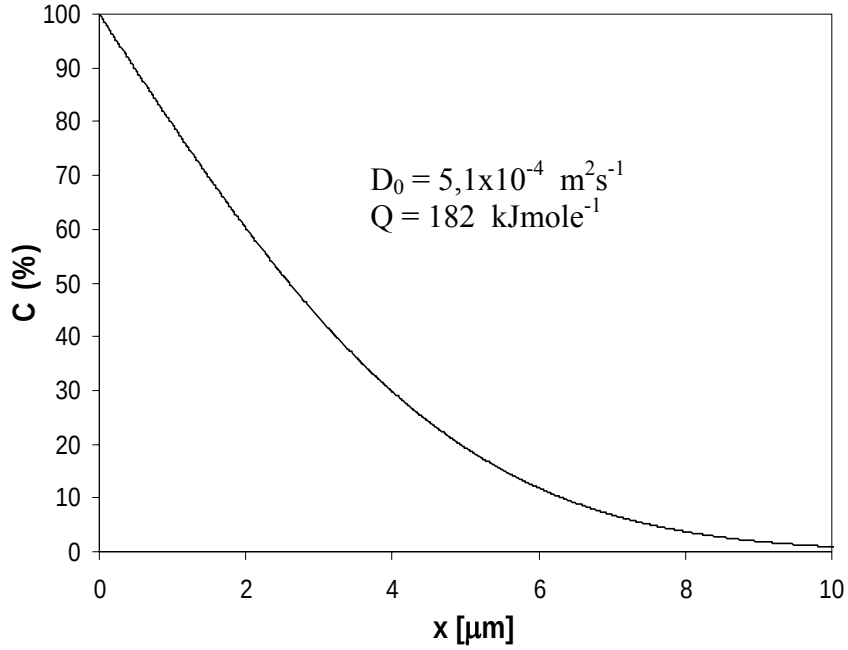

Fig.51 Carbon concentration profile calculated for the heat treatment of 8 h (2.88 × 104 s) at 500 ◦C for the C diffusion in Ti-α;

The same calculation has been performed for the diffusion of carbon in TiC. The values of D_0 and Q, taken from Ref. [33], are displayed in Fig.52 together with the carbon profile. In this case, carbon diffuses over a distance of about 12 nm and the calculated value is in good agreement with the aforesaid experimental value.

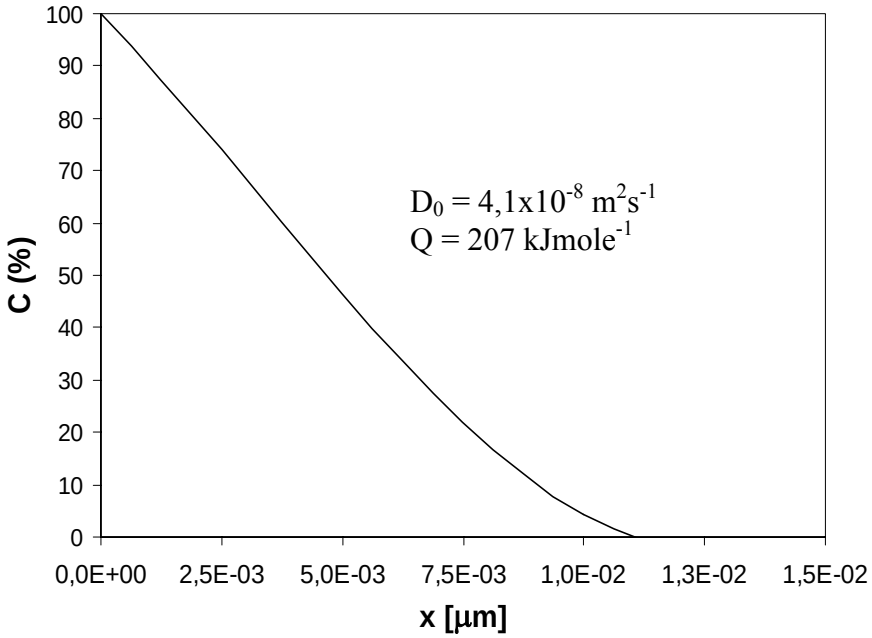

Fig.52 Carbon concentration profile calculated for the heat treatment of 8 h (2.88 × 104 s) at 500 ◦C for the C diffusion in TiC

The comparison between experimental and the calculated data suggests that carbon diffusion in titanium occurs only at the beginning of the process; then carbon combines with titanium to form a TiC layer which separates graphite from metal matrix (as the TEM images indicate in Fig.35, too). The interface growth is governed by the diffusion of carbon in TiC which is much slower than diffusion of carbon in titanium.

The conditions of composite fabrication process involve the formation of TiC layer between carbon and the matrix. Heat treatments in the range of 400-600 °C, of interest for some applications in aeronautical engines, also for prolonged time as those examined here, are not able to induce remarkable modifications of the reaction zone because the diffusion of C through TiC is very slow: so the micro-chemical status remains stable.

IF spectra of composite and alloy show a background which exponentially increases with temperature. The background, which is strongly structure-sensitive [34], is higher for the alloy than for the composite. The result can be explained by considering a different contribution to background from dislocation damping in the two materials: the grain size is near the same in both of them while they have a different dislocation density (calculated by XRD analysis), which is about one order of magnitude higher in the alloy.

About the anelastic phenomena studied to verify the structural stability of the composite under dynamic behaviour, the IF spectrum of the composite shows a Debye peak (at about 870 K) which is not observed in the Ti6Al4V monolithic alloy. Since the peak has been observed also after a prolonged heat treatment at 1073 K, it can not be related to a possible transformation of unstable β phase. Its origin is clearly connected to the presence of the fibres and their effects on the surrounding matrix; for giving an explanation some hypothesis have been considered.

Different phenomena giving rise to energy dissipation may occur at the fibre-matrix interface when composites are subjected to thermal and/or mechanical stresses. At high stresses plastic flow and interface de-bonding may occur, at low stresses matrix and fibres undergo only elastic distortions.

The effects of plastic flow and fibre-matrix de-bonding on modulus and damping have been described and discussed by Schaller [35]. As a consequence of the different values of coefficient of thermal expansion between matrix and fibres internal stresses arise along the production process during cooling from HIP temperature (1163 K) to room temperature. However, a simple calculation shows that the stresses are not sufficiently high to induce the formation of dislocations in the matrix near the fibres. The mean stress α_M in

the matrix arising from cooling from HIP temperature (T_{HIP}) to room temperature (T_R) can be expressed by:

$$\sigma_M = \frac{E_F E_M}{(E_F \phi + E_M (1-\phi))} \phi(\alpha_M - \alpha_F)(T_{HIP} - T_R) \tag{5}$$

where E_F , α_F and E_M , α_M are the Young's modulus and the coefficient of thermal expansion of fibre and matrix respectively, ϕ the volume fraction of fibres. Introducing in eq.(5) the values E_F = 400 GPa, E_M = 114 GPa, α_M = 9.6 x 10^{-6} K^{-1}, α_F = 4.1 X 10^{-6} K^{-1} and ϕ = 0.3, σ_M = 350 MPa has been obtained. This value is much lower than the yield stress of matrix σ_Y = 850 MPa. Furthermore, dynamic modulus and Q^{-1} at room temperature do not change after repeated test runs on the same sample. Therefore, plastic flow and de-bonding at the fibre-matrix interface have been ruled out as a possible cause of the anelastic phenomena observed by us and the attention has been focused on elastic strains at the interface.

This condition has been analysed by He and Lim [36] on the basis of the interfacial diffusion mechanism [37]. When a shear stress is applied, the interface, which is not perfectly planar on a microscopic scale, is under tension at some locations and under compression at some others (Fig.53).

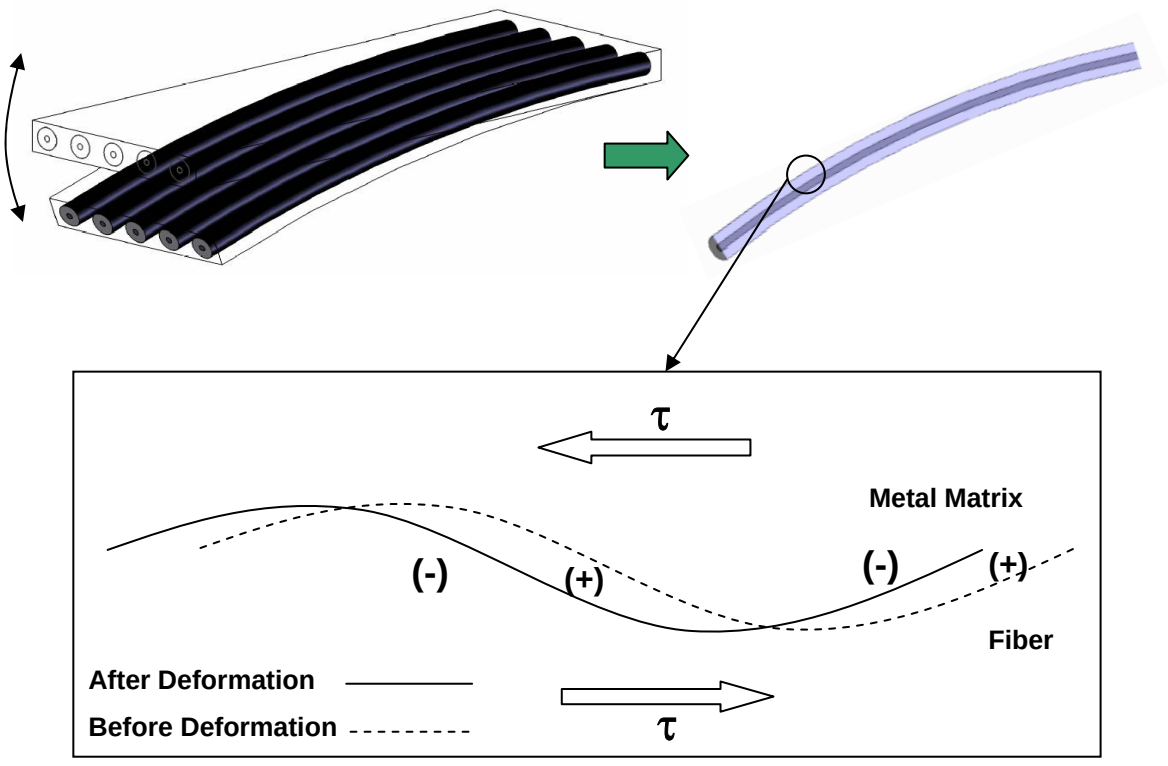

Fig.53 Studied mechanism to verify the phenomena about the obtained IF peak. (+) *Traction strain,* (-) *compression strain.*

The stress gradient induces atom diffusion along the interface causing anelastic behaviour. However, the activation energy determined from our experiments, H = 186 kJ/mole, is quite different from those controlling the atomic diffusion of Ti, Al and V in both α and β phases present in the matrix thus the IF peak can not be ascribed to such mechanism. Also diffusion processes inside the fibres, which have a stratified axial-symmetric structure, are not compatible with the peak activation energy.

As shown, the SiC fibres are coated by a carbon layer (thickness ≈ 3 μm) which separates SiC from Ti6Al4V matrix. During the process of composite fabrication, carried out at high temperature (1163 K), carbon reacts with titanium forming a thin layer (few nanometers thick) of titanium carbide (TiC). TiC thickness grows when the material is heat treated but the kinetics is very slow. The activation energy for TiC growth, independently determined by Naka et al., is 194 kJ/mole, close to that of IF peak. Therefore, the peak seems somehow connected to the growth of the TiC layer between fibre carbon coating and the matrix. Furthermore, one has to consider that its activation energy is in fact very close to that of carbon diffusion in the α–Ti (H* = 182 kJ/mole). On these grounds, it is believed that the peak is due to stress induced reorientation of interstitial-substitutional (i-s) pairs (C-Al and C-V) in the hcp α phase of the matrix near the fibres where the formation of TiC produces a zone richer of substitutional atoms than the remaining matrix (Fig.54). The mechanism has been discussed by Gupta & Weining [38] and Povolo & Bisogni [39] for hcp metals.

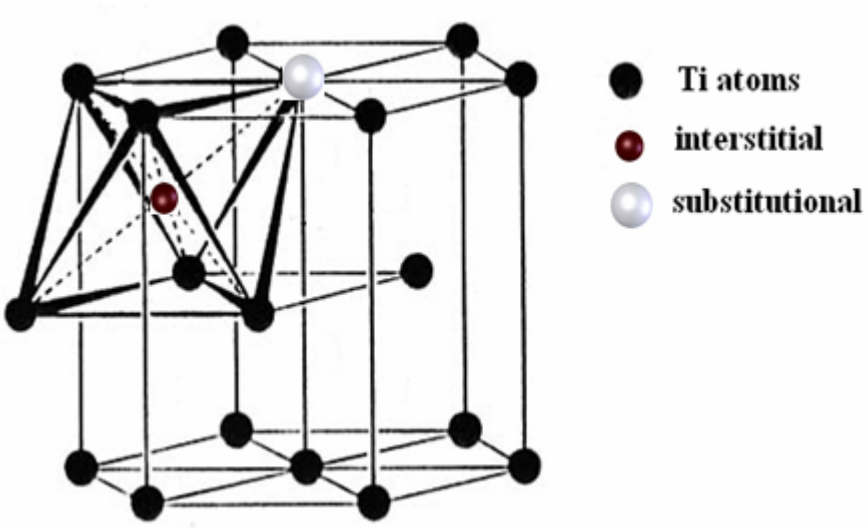

Fig. 54 Interstitial- substitutional (i-s) pair in the h.c.p. lattice of the composite α phase.

The comparison between the internal friction probes carried out about the two different typologies of the composite has showed very similar trend. In fact about the

composite produced by *Roll Diffusion Bonding* it is possible to observe a relaxation peak at about 600°C, too. This latter results having an higher background, due to the more important presence of the dislocations, based to the aforesaid concepts about the role of dislocation density. Moreover about the analysis of the observed relaxation phenomena, the resulting found peak can be interpolated very well by a Debye peak. By this way it has been possible to calculate the value of activation energy, that results very much close to the value for the *HIP* composite, confirming the fundamental role of the fiber presence about the anelastic phenomena that develop.

About this micro-chemical an micro-structural concepts and about the founded difference between the two composite typologies, a last consideration mast be developer by the metallographic analysis: in fact these verify a finer structure for the *RDB* composite, but other developing should be carried out to make clear the importance of the micro-void observed on the junction zones near the fibers.